8-1-1988

A Chamfered Connection for Use in Automated Framing of Buildings

V. X. Nguyen

N. D. Perreira

ADVANCED TECHNOLOGY FOR LARGE
STRUCTURAL SYSTEMS

Lehigh University

A CHAMFERED CONNECTION FOR USE IN AUTOMATED FRAMING OF BUILDINGS

by

V.X. Nguyen
and
N.D. Perreira

ATLSS Report No. 88-06
August 1988

An NSF Sponsored Engineering Research Center

ADVANCED TECHNOLOGY FOR LARGE STRUCTURAL SYSTEMS

Lehigh University

A CHAMFERED CONNECTION FOR USE IN AUTOMATED FRAMING OF BUILDINGS

by

V. X. Nguyen

and

N. D. Perreira

Lehigh University

August 10, 1988

This report was adapted from a thesis that was accepted and approved in partial fulfillment of the requirements for the degree of Master of Science for Mr. Nguyen in May 1988.

Table of Contents

1	Abstract	1
2	Introduction	2
3	System Analysis	6
4	First Stage	21
	4.1 Geometrical Analysis	21
	4.2 Force and Moment Analysis	29
	4.3 Trajectory	38
5	Second Stage	42
	5.1 Geometrical Analysis	42
	5.2 Force Analysis	44
	5.3 Moment Analysis	53
	5.4 Trajectory	55
6	Conclusions	61
7	List of References	65

1. ABSTRACT

Automated erection of building frames involves the use of handling systems and connection technologies. A new connection-making mechanism is one of the efforts being developed to facilitate the framing task. The results of this study are used in defining the design constraints on handling system capable of erecting building frames.

A particular type of "chamfered" connection is studied in this paper. First, the connection geometry parameters are determined. Second, possible trajectories of the beam-column system are observed. Third, forces and moments acting on the handling system during the insertion process are derived. Finally, the stiffness of the connection is obtained.

It was found that the connection geometry parameters greatly affect the maximum allowed amount of initial misalignment between the beam and the column. They also affect the forces, the moments acting on the beam and the handling systems, as well as the stiffness of the connection.

2. INTRODUCTION

The use of robotics technology within construction is recently gaining a great deal of attention. The main thrusts behind the use of this technology are to increase the safety of the workers, to ensure consistent quality of construction, and improve productivity. Research in construction automation and robotics is concentrated on various activities that occur within the phases of construction. This paper investigates one aspect of applying a new connection design within the inserting activity of the framing phase; the case of insertion. This aspect is crucial to automating the erection of steel and steel reinforced structures.

The framing, or erection phase is where the skeleton of a building is assembled. Frames may be composed of various materials, ranging from reinforced concrete to steel to wood. Erection includes the subtasks or activities of identifying and locating the structural members at the staging area; slinging, hoisting and positioning the frame elements to their destination; aligning, inserting and connecting the joints of the elements; and then guiding and aligning the frame. With the current assembly method, a lot of time and labor is spent during the final positioning of the girder at the connection points. Any misalignment

between the columns and the girder has to be corrected by the steel workers, so the holes will be matched for bolting or the edges will be matched for welding. The process is so dependent on the tolerance that in many cases, either the column or the girder has to be modified so they can fit together [1].

One of the approaches to reduce the efforts required within the erection process is to design the elements for erectability in ways similar to how one now designs manufacturing components. One particular connection, the "chamfered" connection, is studied in this paper. This connection was initiated by the well known peg and hole problem [5]. The knowledge of the peg and hole problem will be used to guide the study as well as to understand the results obtained. With a "chamfered" connection, the misalignment between the columns and the beam is self corrected by the design. The beam and the columns are also locked together after they are mated, thus no temporary support or securing is necessary. Moreover, it has been found in automated manufacturing systems that the appropriate choice of connection will decrease the complexity required of the robotic equipment and sensors [3]. The use of these connections should also greatly reduce the effort required to plumb the erected structure. These four

advantages will significantly reduce the time, the labor and the cost of the framing phase.

Several goals are achieved in this study. First, with a set of initial relative position and orientation errors between the desired and achieved beam destination, a combination of dimensional parameters to have a successful assembly is found. Second, the forces and moments acting on the beam during the process are determined using force and moment balance equations. This information may be used in the design and selection of the equipment used to handle the beam. For example, some of the requirements for the use of a tower crane robot arm are determined. Third, the stiffness of the connection at different stages of the insertion process is obtained by combining the force equations with kinematic constraint equations. The constraint equations describe the relationship between the connection geometry and allowable positions and orientations of the beam relative to the columns. A good connection design will produce a low stiffness so that less power and a less rigid robot arm are required to drive the beam into its desired position. Finally, the trajectory of the beam during the insertion process will be determined.

This paper examines a particular yet representative insertion trajectory. In section 3 the system

components are described. The identification of all possible contacts is presented and trajectories between these contacts are given in a table. A particular trajectory is selected for detailed analysis, and is separated into a number of stages. The analysis of the first and the second stage is presented in sections 4 and 5. Section 7 discusses and generalizes the results of the study.

3. SYSTEM ANALYSIS

The connection consists of a "chamfered foot" and a "chamfered shoe" as shown in Fig.1. The foot is guided through the insertion process by the chamfers and is locked within the shoe at the end of the insertion by a wedging effect. An additional lock can be supplied by bolting. The shoe and the foot are not initially incorporated in the beam or the column when they leave the mill. They are fabricated pieces either welded or bolted on to beams, girders and the columns at the fabrication shop prior to being sent to the erection site.

The system being analyzed consists of two rigidly supported shoes a distance apart and a beam and two feet as shown in Fig.1. Two coordinate systems are used within the analysis. The "shoe coordinate system" is fixed in space and located at the corner O of the left shoe. The "foot coordinate system" is located at the centroid of the beam. This coordinate system moves with the beam during the insertion process.

The analysis considers both a single sided insertion and a two sided insertion. In a single sided insertion, we only investigate the interaction between one foot and one shoe on one end of the beam. In the two sided insertion, interaction between both feet of the beam and both shoes of the columns will be studied.

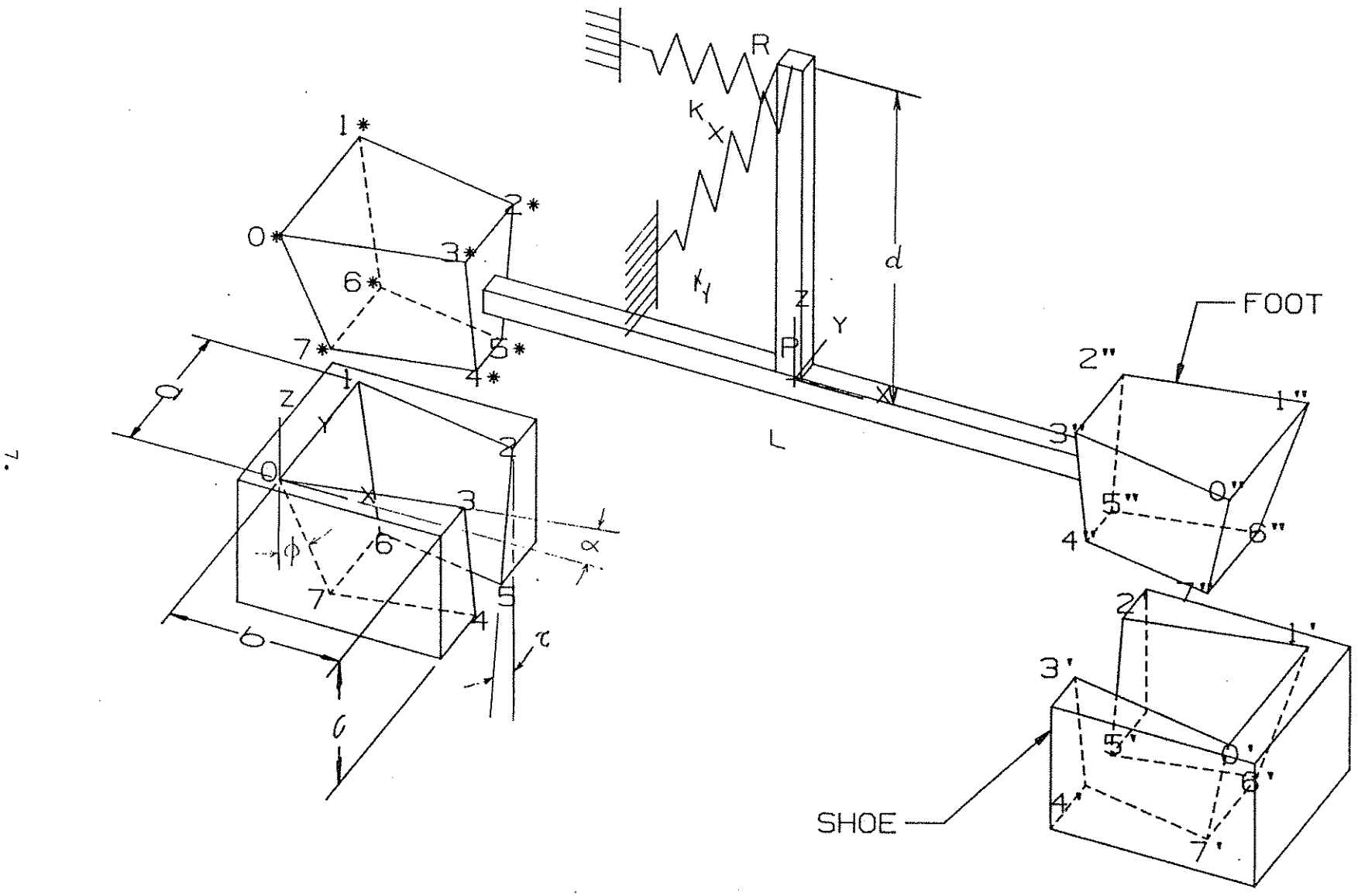

FIG. 1 : NOMENCLATURE AND DEFINITIONS

Single sided insertion. This class of insertion is similar to the simple peg and hole problem [5] except that multiple types of contacts and insertion trajectories are possible. The type of contact that occurs depends on how the foot is located relatively to the shoe. The first contact made can belong to one of seven groups: one-point, two-point, three-point, line, line-(one-point), line-(two-point), or (two line)-(one-point) contact. The seven groups are shown in Table 1. Each of these groups has a number of various types, in total of thirty nine different contact types are possible. Each contact is given an identification number and drawn in Figs.2-7.

Table 2 demonstrates the successive moves between different contact types during a typical insertion process. The table is constructed based on the observation of a model with a particular set of parameters. The general nature of insertion over all geometric parameters has not been determined. Each column within the table represents a sequence of moves during an insertion and defines a class of trajectory. The first number in any column identifies the starting contact type. The second number identifies the next type of contact that will be encountered. The column describes all steps of an insertion terminating at the final "goal", or when the foot and the shoe are perfectly matched. For example, point contact #31 can develop into one of the

TYPE	#'S OF CONTACTS	I.D.
POINT	5	1, 2, 16, 31, 53
2 POINT	8	12, 14, 32, 33, 34, 35, 41, 42
3 POINT	5	24, 36, 39, 43, 44
LINE	5	6, 8, 10, 5, 9
LINE-POINT	6	18, 20, 22, 37, 48, 49
LINE-(2 POINT)	9	26, 28, 30, 40, 45, 47, 50, 51, 52
2 LINE-POINT	1	38

TABLE 1: TYPES OF CONTACTS

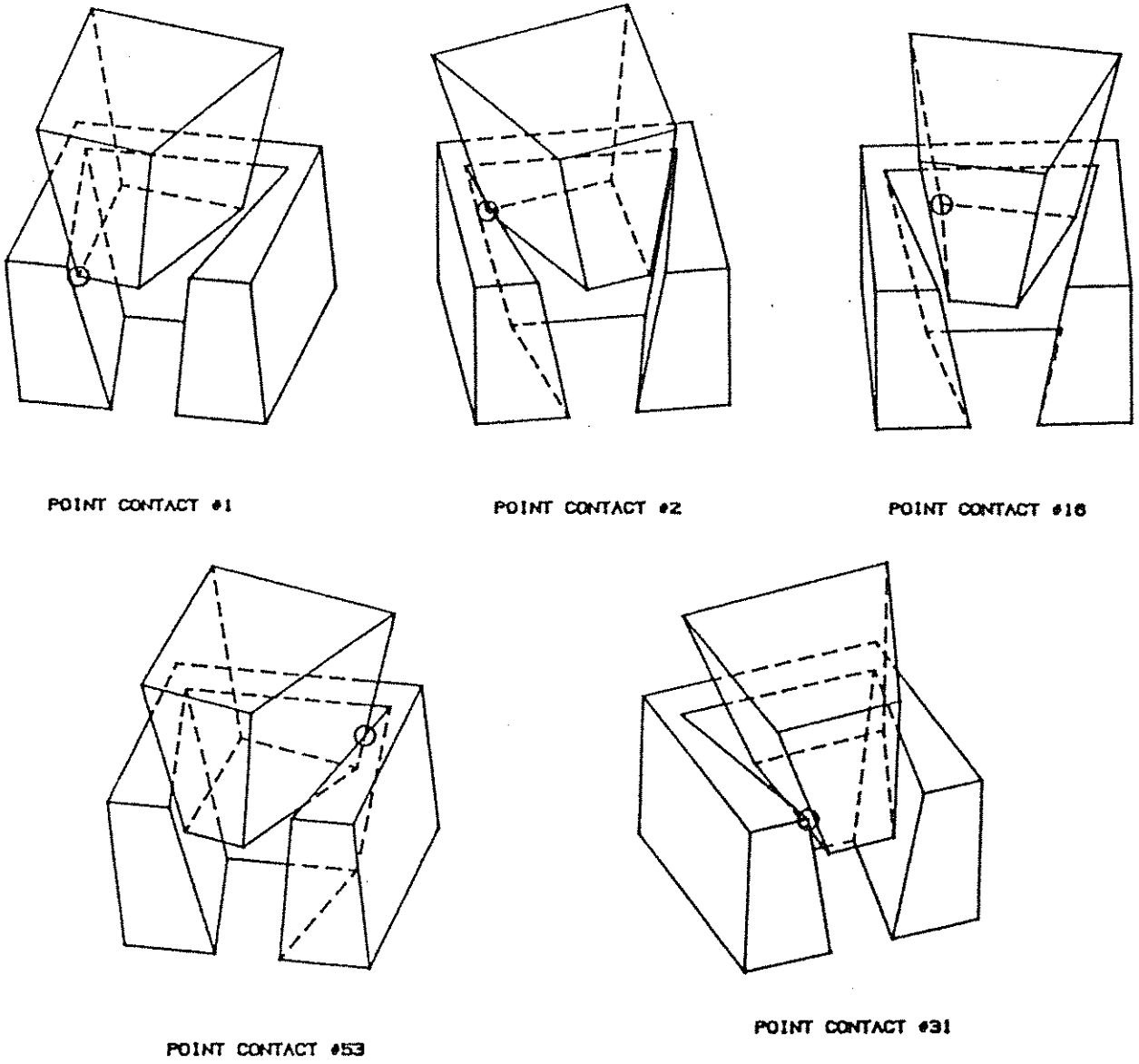

Fig.2 : One Point Contact Group

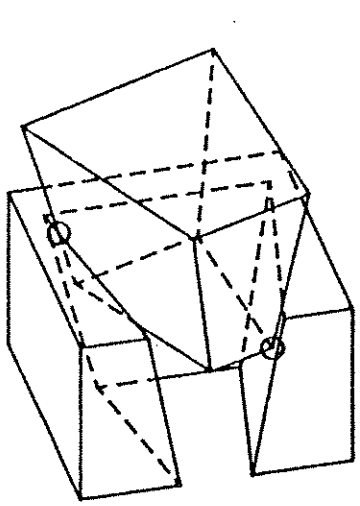

2 POINT CONTACT (#12)

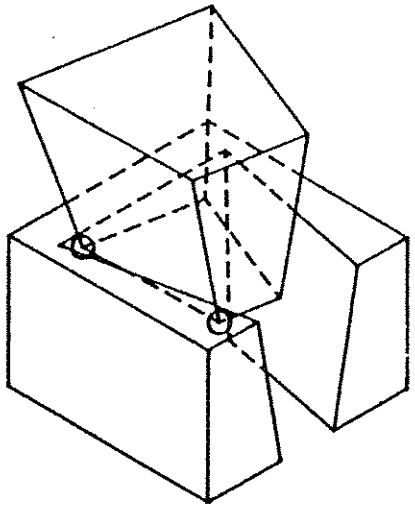

2 POINT CONTACT (#14)

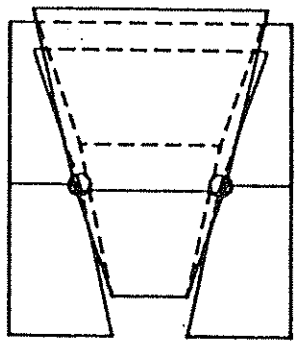

2 POINT CONTACT (#32)

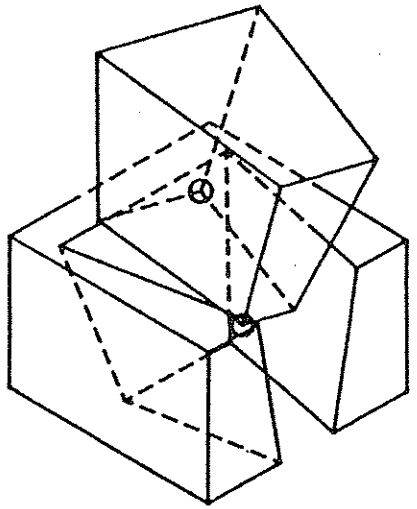

2 POINT CONTACT (#33)

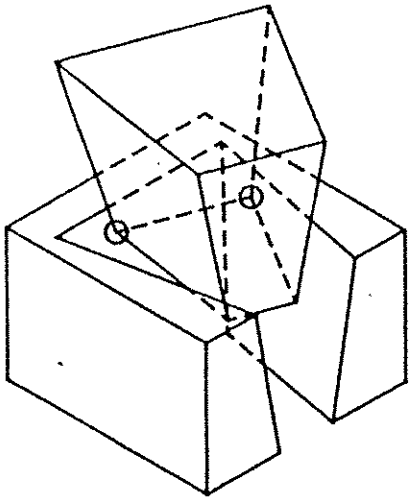

2 POINT CONTACT (#34)

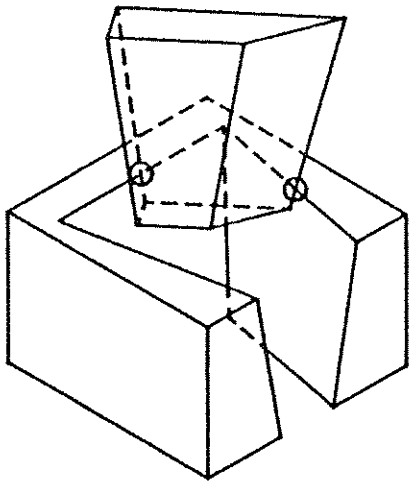

2 POINT CONTACT (#35)

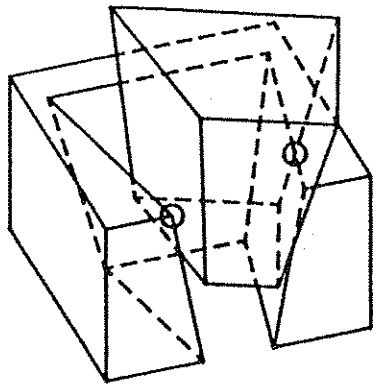

2 POINT CONTACT (#41)

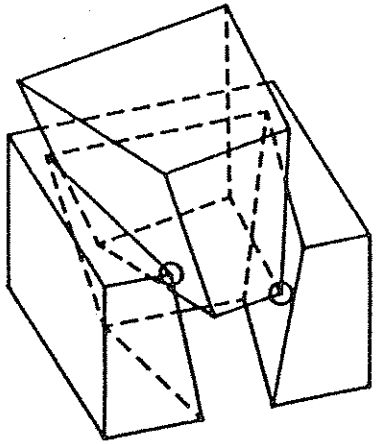

2 POINT CONTACT (#42)

Fig.3 : Two-Point Contact Group

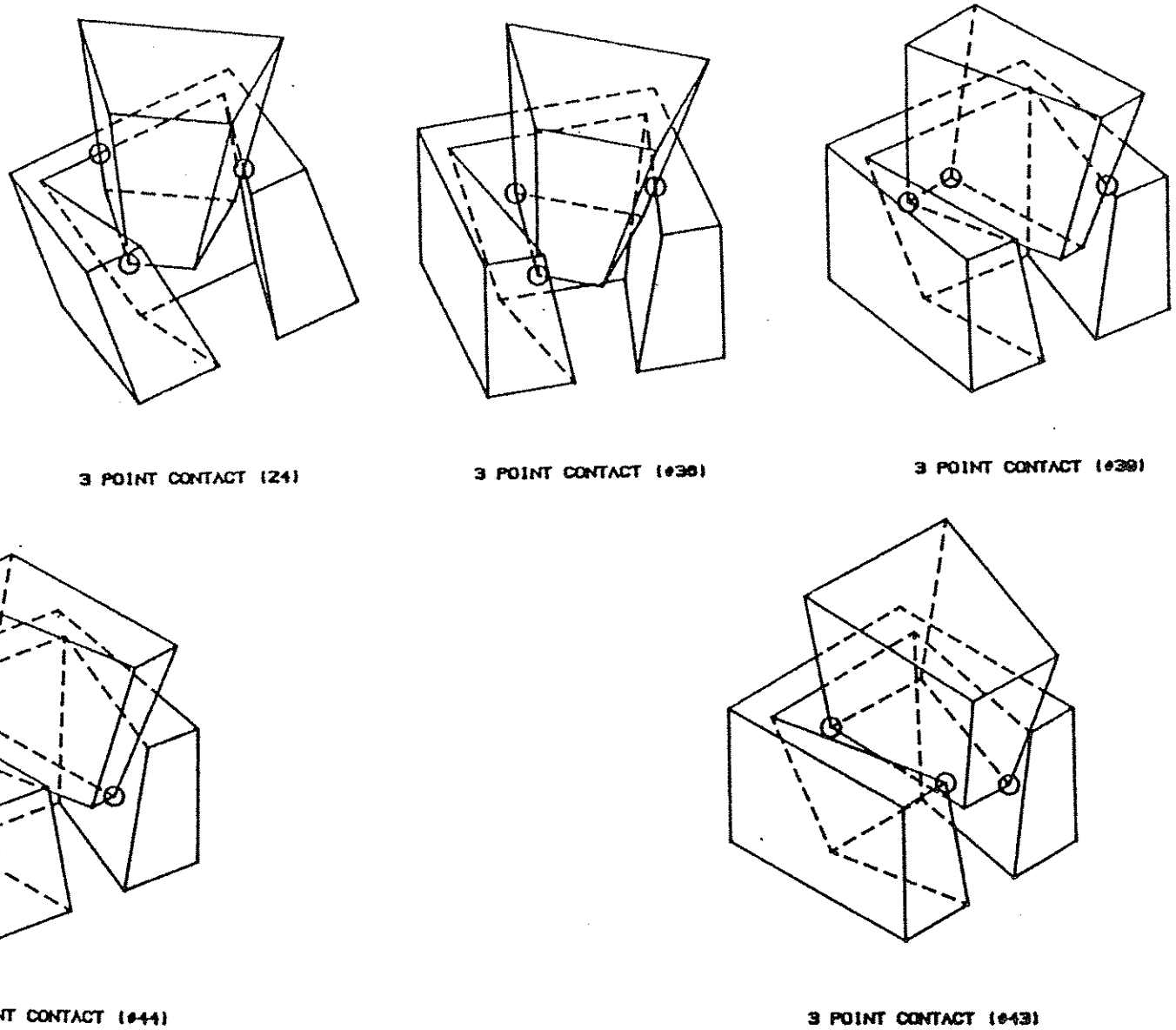

Fig.4 : Three-Point Contact Group

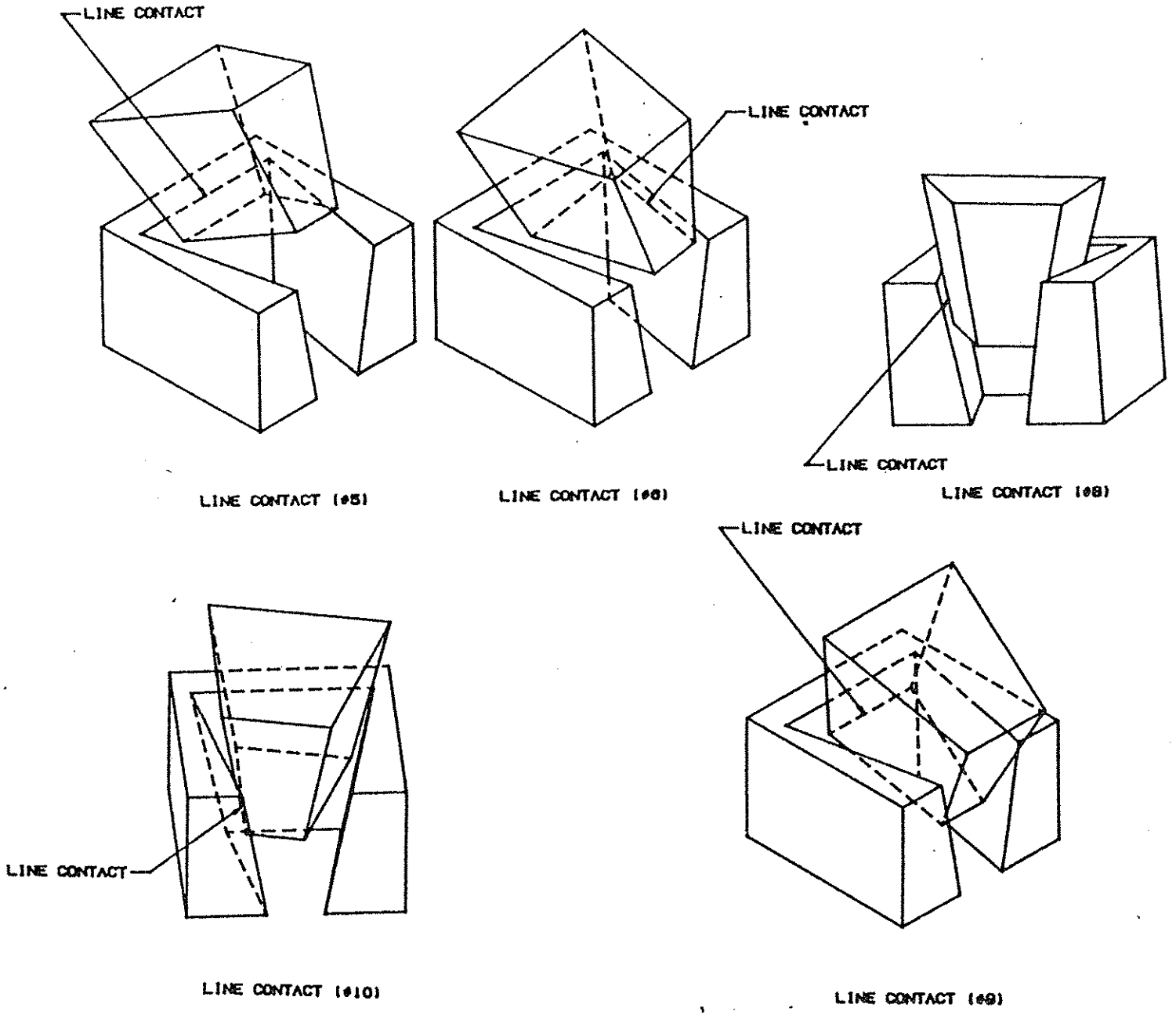

Fig.5 : Line Contact Group

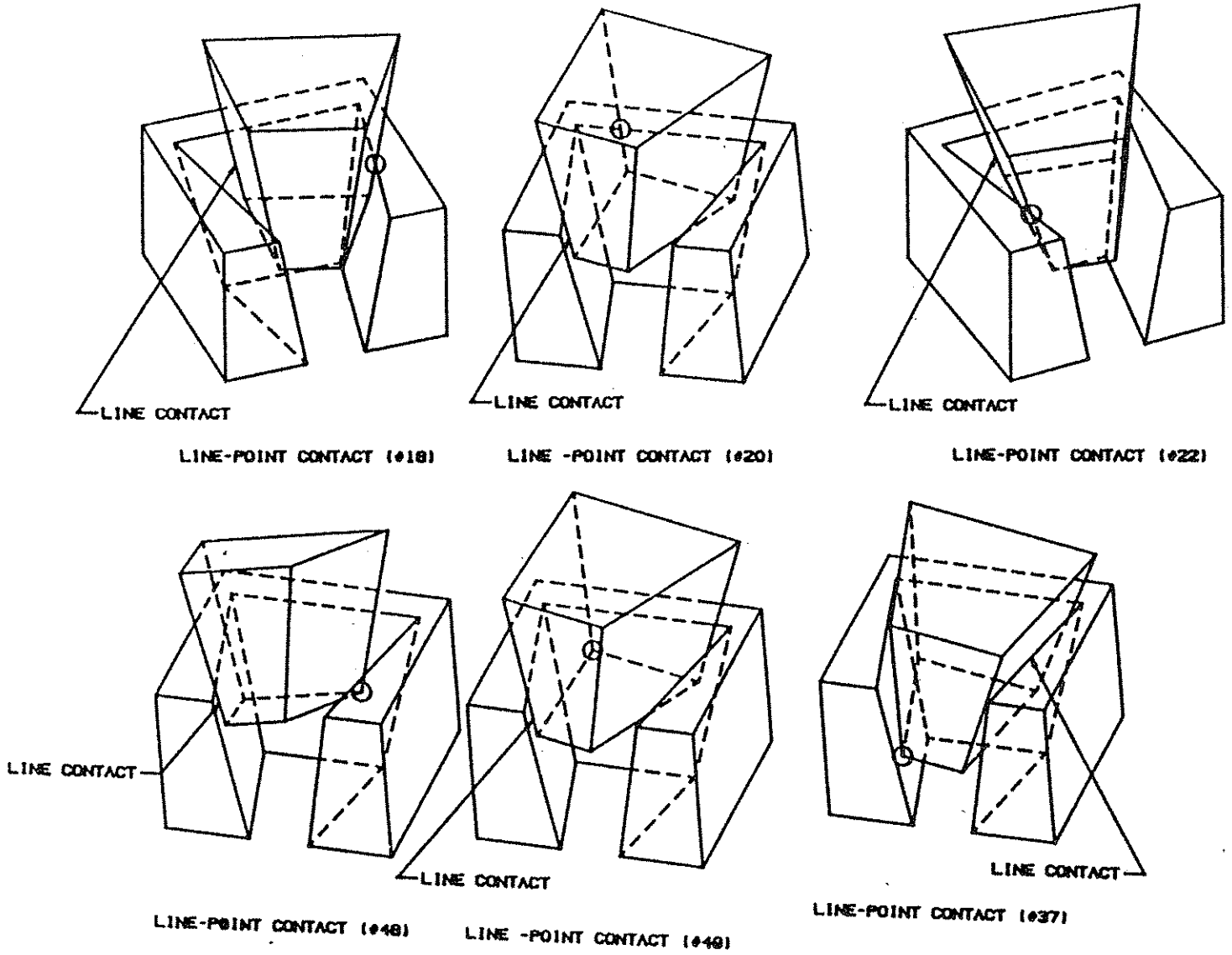

Fig.6 : Line-Point Contact Group

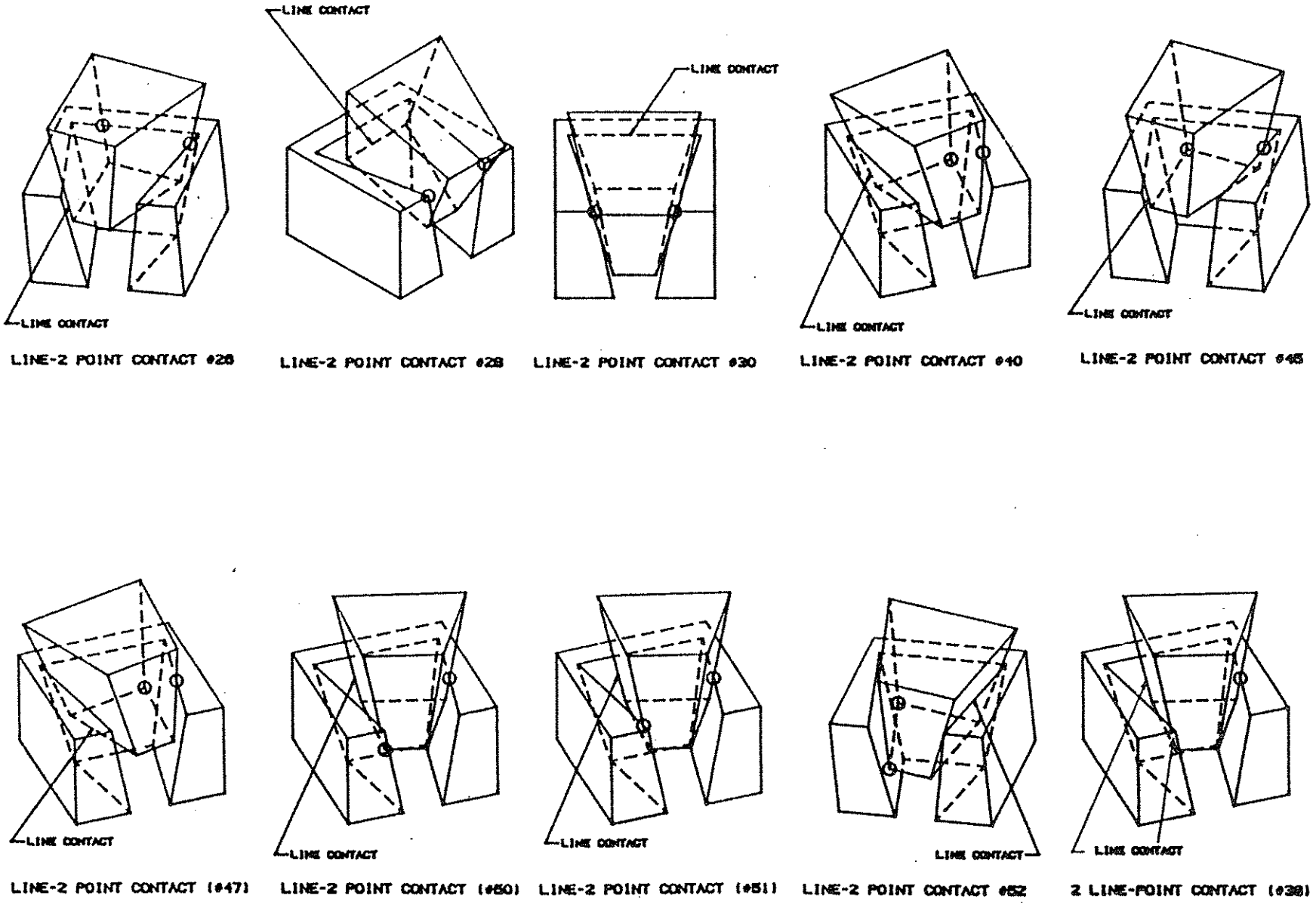

Fig.7 : Line-Two Point and Two Line-Point Groups

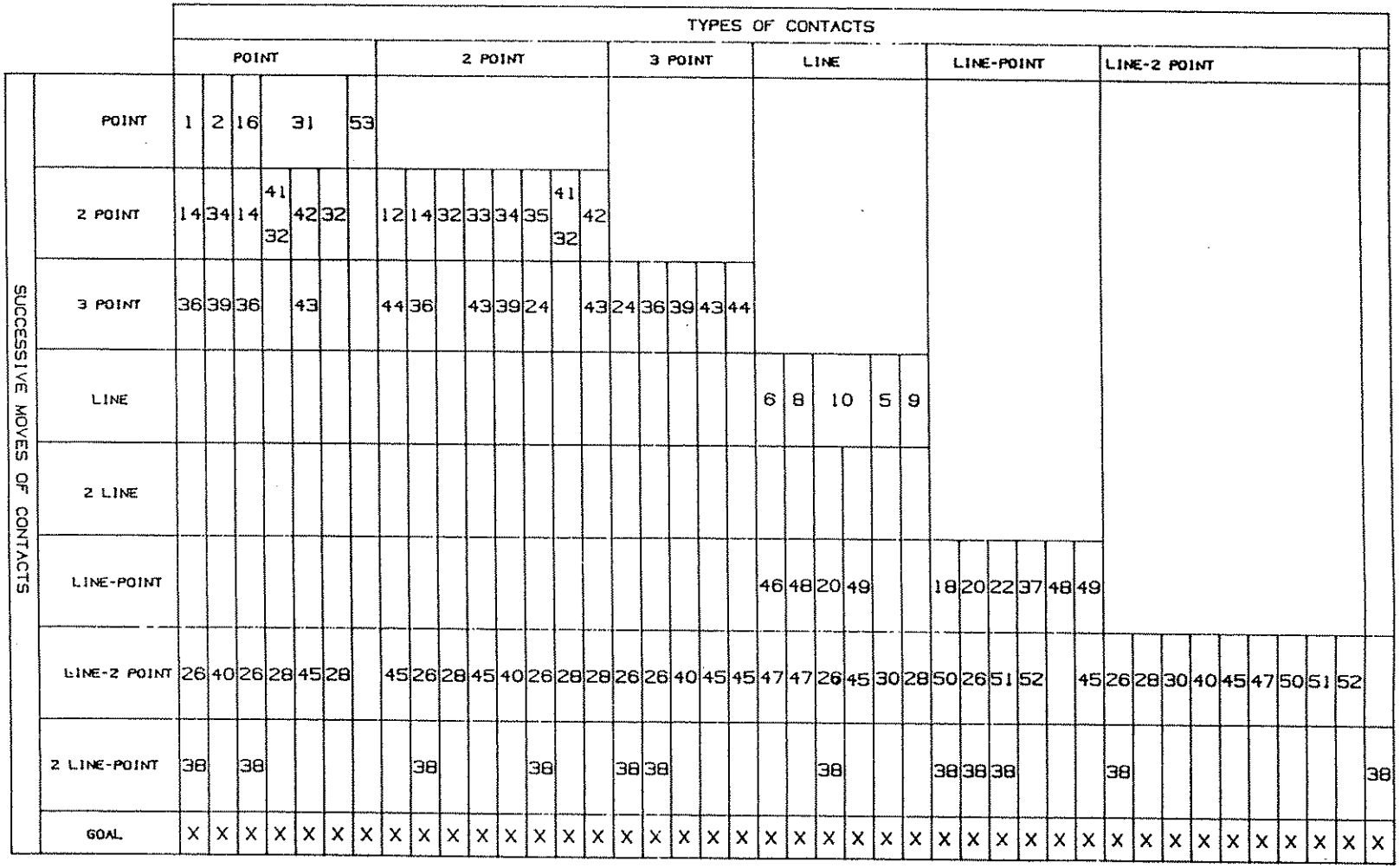

TABLE 2: SUCCESSIVE MOVES OF CONTACTS

three following move patterns: 31-41-32-28 or 31-42-43-45 or 31-32-28.

Two sided insertion. Beam-column insertions are composed of simple one sided insertion and the complex two sided insertion where the simultaneous insertion of two feet into two shoes occurs. The misalignment between the beam and the column members dictates which side the beam will engage first and what type of contact will occur. In the most common assembly, single sided insertion will first occur. Further insertion of the beam will initiate a contact on the other side of the beam. As the insertion process continues, contact trajectories will proceed at each end of the beam. Typically the class of contact trajectories will differ. As the beam is inserted, the misalignment of the system components is reduced.

We will concentrate only on a specific move pattern, which we believe to be representative of the beam to column insertion process. The move pattern under study starts with the beam above the column members (Fig.7a). The column shoes are assumed fixed throughout the insertion and tolerancing and assembly errors are assumed negligible. The beam is initially placed above the shoes with an angle error around the Z_F axis of δz and position errors in the x and y directions of dx and dy. As the beam is inserted, it will first make a one-point contact, #16, at its left end. This begins stage 1 of the insertion process. As the beam

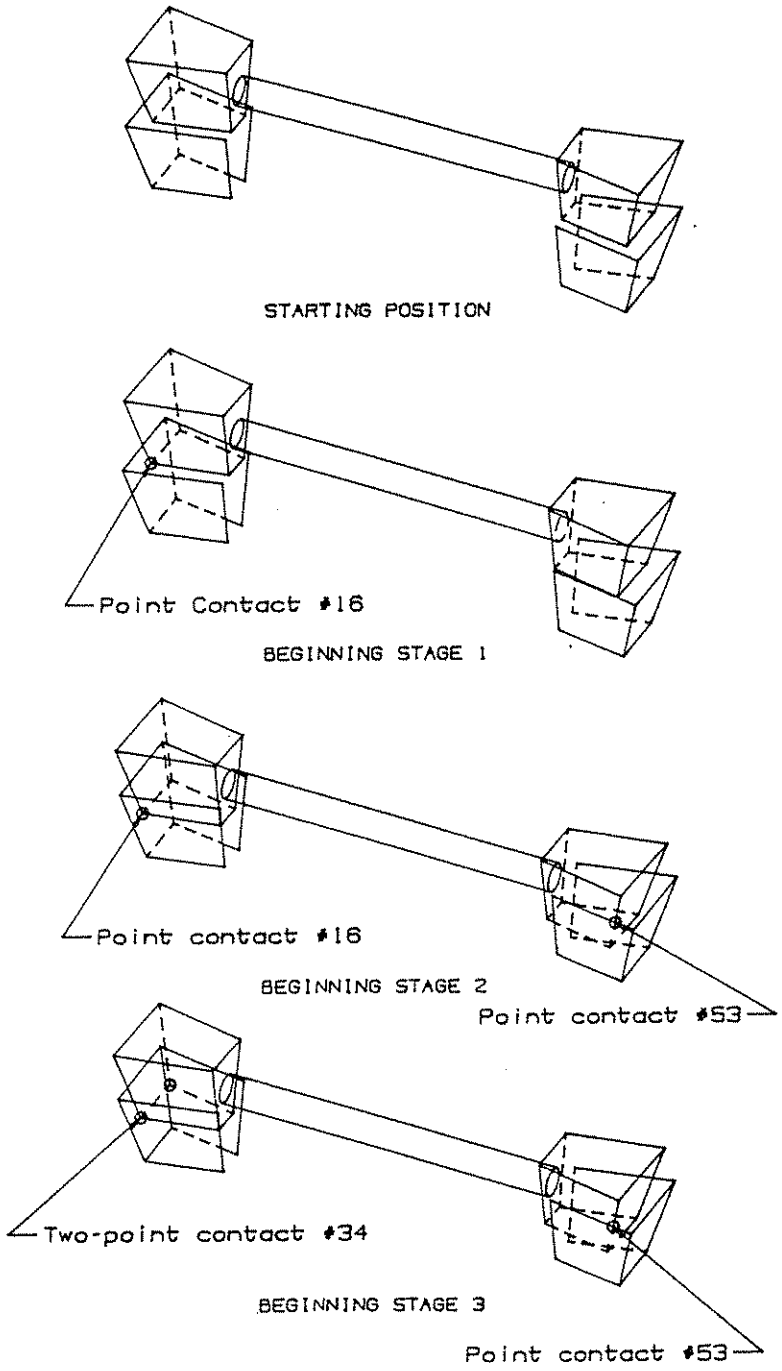

Fig. 7a : The Studied Trajectory

continues to go down, a second one-point contact,#53, on the right end will occur. This begins stage 2 of the insertion process. The system maintains that mating fashion until two-point contact,#34, is initiated on the left. This begins the third stage of the insertion process. The following analysis concentrates on the first two stages. The latter stages can be analyzed, using similar analysis techniques.

The beam is supported above its centroid at point R by compliant interface between the beam and its handling system is shown in Fig. 2. The compliance is used in determining the required compliance of the handling system. The handling system could be a tower crane, a robotic arm or similar system. The interface could include an RCC device. Both translation and rotation compliance are provided by the interface in order to properly mate the beam with the columns as well as support and force the beam down the shoes. The translational compliance is supplied by two springs attached at point R with the spring constants K_x and K_y. The rotational compliance is provided by a torsional spring with the spring constant k_θ also mounted at R and not shown in the Figure. We assume that the handling system will not allow the beam to rotate around X_f axis and Y_f axis.

The two stages of the insertion process will be examined in order of occurrence. Small angle

approximations are used, explicit solutions are obtained and several interesting properties are derived and studied. Geometrical parameters of the shoe, the foot and the beam being examined include a,b,c,α,τ,ϕ,L, whereas "error parameters" include dx, dy and δz. Acceptable combinations of all parameters required for a successful sequence of movements as described above are determined. Using those parameters determined all the forces and moments required for the insertion are K. The compliance of the connection and the resulting trajectory of the beam are also derived.

4. FIRST STAGE

This section is organized as follows: first the geometrical analysis is carried out to determine the right combination of the design parameters to have a good insertion. Second, all the forces and moments acting on the handling system are derived from the force and moment balance equations. Finally, the stiffness of the connection and the trajectory are obtained.

4.1 GEOMETRICAL ANALYSIS

Two preliminary geometric requirements must be met to achieve a successful insertion. First the foot must be so aligned as to engage the chamfer of the shoe. The alignment is further restricted to a region where a stable insertion process can occur.

First condition. The insertion will fail if any of the four bottom corners of the feet are outside of the mating portion of the shoes as shown in Fig.8. To avoid such a failure, combinations of acceptable geometrical parameters can be determined for any specific set of maximum initial beam placement errors.

The analysis requires determining the locations of the four corners of the feet in terms of the shoe coordinate system and then checking if they lay within an acceptable

region created by the appropriate four parameter points of the shoes.

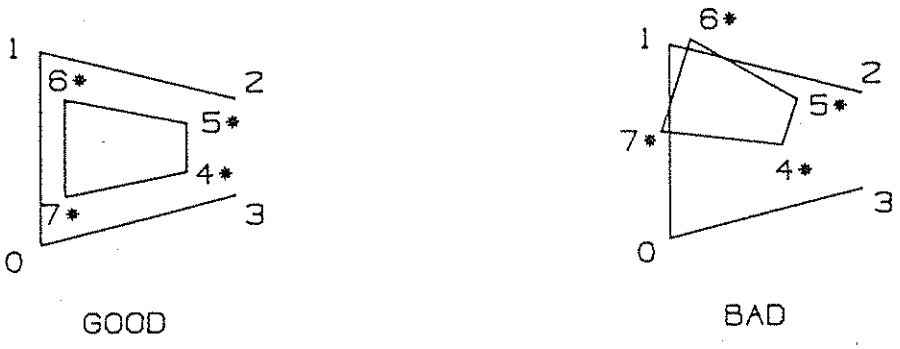

Fig.8 : Good and bad starting positions

The coordinates of all the corners of the shoes in the shoe coordinate system are obtained by trigonometry and presented in Table 3, while the coordinates of the feet in the foot coordinate system are tabulated in Table 4.

We then determine the coordinates of the corners of the feet in the shoe coordinate system . This is done for initial beam positions which are taken at a rotation of δz about the beam Z axis and at distances dx and dy in the X and Y direction respectively. The following transformation is used:

Point	Coordinates		
	x	y	z
0	0	0	0
1	0	a	0
2	b	a-btanα	0
3	b	btanα	0
4	b	btanα+ctanτ	-c
5	b	a-btanα-ctanτ	-c
6	ctanϕ	a-c(tanτ+tanαtanϕ)	-c
7	ctanϕ	c(tanτ+tanαtanϕ)	-c
0′	l+2b	0	0
1′	l+2b	a	0
2′	l+b	a-btanα	0
3′	l+b	btanα	0
4′	l+b	btanα+ctanτ	-c
5′	l+b	a-btanα-ctanτ	-c
6′	l+2b	a-c(tanτ+tanαtanϕ)	-c
7′	l+2b	c(tanτ+tanαtanϕ)	-c

Table 3: Coordinates of corners of the shoe in the shoe coordinate system.

Point	Coordinates		
	x	y	z
0*	$-((L/2)+b)$	$-a/2$	$c/2$
1*	$-((L/2)+b)$	$a/2$	$c/2$
2*	$-L/2$	$a/2-b\tan\alpha$	$c/2$
3*	$-L/2$	$-(a/2-b\tan\alpha)$	$c/2$
4*	$-L/2$	$b\tan\alpha+c\tan\tau-(a/2)$	$-c/2$
5*	$-L/2$	$-(b\tan\alpha+c\tan\tau-(a/2))$	$-c/2$
6*	$(-L/2)-b+c\tan\phi$	$(a/2)-c(\tan\tau+\tan\alpha\tan\phi)$	$-c/2$
7*	$-(L/2)-b+c\tan\phi$	$-((a/2)-c(\tan\tau+\tan\alpha\tan\phi))$	$-c/2$
0"	$(L/2)+b$	$-a/2$	$c/2$
1"	$(L/2)+b$	$a/2$	$c/2$
2"	$L/2$	$(a/2)-b\tan\alpha$	$c/2$
3"	$L/2$	$-((a/2)-b\tan\alpha)$	$c/2$
4"	$L/2$	$b\tan\alpha+c\tan\tau-(a/2)$	$-c/2$
5"	$L/2$	$-(b\tan\alpha+c\tan\tau-(a/2))$	$-c/2$
6"	$(L/2)+b-c\tan\phi$	$(a/2)-c(\tan\tau+\tan\alpha\tan\phi)$	$-c/2$
7"	$(L/2)+b-c\tan\phi$	$-((a/2)-c(\tan\tau+\tan\alpha\tan\phi))$	$-c/2$

Table 4: Coordinates of feet corners in the foot coordinate system.

$$[x_p-dx \quad y_p-dy \quad z_p] + [x_b \; y_b \; z_b] \begin{bmatrix} \cos\delta z & -\sin\delta z & 0 \\ \sin\delta z & \cos\delta z & 0 \\ 0 & 0 & 1 \end{bmatrix} \quad (1)$$

where:

$x_p = (L/2)+b$, $y_p = a/2$ and z_p is the z coordinate of the beam centroid P anywhere above the beam in the shoe coordinate system

$[x_b \; y_b \; z_b]$ are the coordinates of the corners of the feet in the beam coordinate system.

The initial coordinates of point 7*, $x_{7*a}, y_{7*a}, z_{7*a}$, are thus obtained from equation (1):

$$x_{7*a} = (x_p-dx)+x_{7*f}\cos\delta z+y_{7*f}\sin\delta z$$

$$y_{7*a} = (y_p-dy)-x_{7*f}\sin\delta z+y_{7*f}\cos\delta z$$

$$z_{7*a} = z_{7*f}+z_p$$

Similar expressions for 4*a,5*a,6*a,4"a,5"a,6"a,7"a are derived from equation (1). For the bottom of the feet not to hit the top surfaces of the shoes requires that the corners of the feet all lay within the region created by the top edges of the shoes as represented in Fig.9 and

$$y+(\tan\alpha)x-a < 0$$

$$x > 0 \quad (2)$$

$$y-(\tan\alpha)x > 0$$

whereas for the right foot the region is given by:

$$x < L+2b$$

$$y+(\tan\alpha)x-(\tan\alpha)(L+2b) > 0 \qquad (3)$$

$$y-(\tan\alpha)x+(\tan\alpha)(L+2b)-a > 0$$

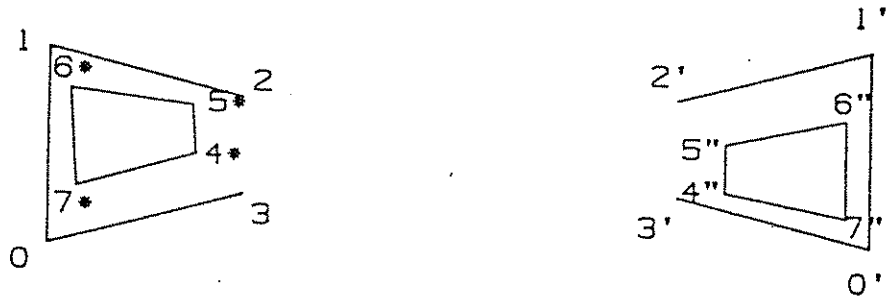

Fig.9 : Boundary Conditions on the Shoes

The various values for the seven geometrical variables determine the range of acceptable initial pose errors.

For example, with the geometric parameters of a=8", b=4", c=12", l=20ft, α=9°, τ=14°, ϕ=9°, the following ranges of initial error variables are obtained:

δz,deg	Ranges of dx, in.	Ranges of dy, in.
0	-1.9 to 1.9	-2.6 to 2.6
0.1	-1.8 to 1.8	-2.4 to 2.4
0.2	-1.7 to 1.8	-2.3 to 2.2
0.3	-1.6 to 1.5	-2.1 to 2

Second condition. A second, more restrictive condition occurs as the foot is placed within the shoe. The relative pose of these two parts in this case is shown

in Fig.10. In both of the two cases, the beam has been rotated clockwise relative to the shoes. In the first of the two cases, x_{7*f} in the shoe coordinate has a positive value. Due to geometrical considers, attempts to insert the feet will result in further clockwise rotation. In the second case, x_{7*f} has a negative value in the shoe coordinate system.

The angle error δz will be reduced as the insertion process proceeds. The second and stable case is obtained if δz, the initial insertion angle is less than δ_{max} which is determined by:

$$\delta_{max} = \frac{y_{7*f}}{x_{7*f}}$$

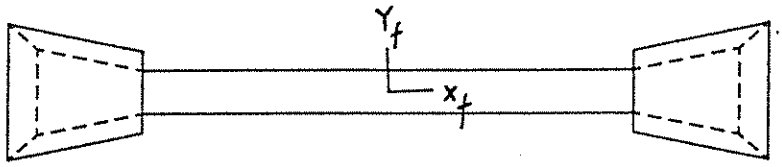

Starting position

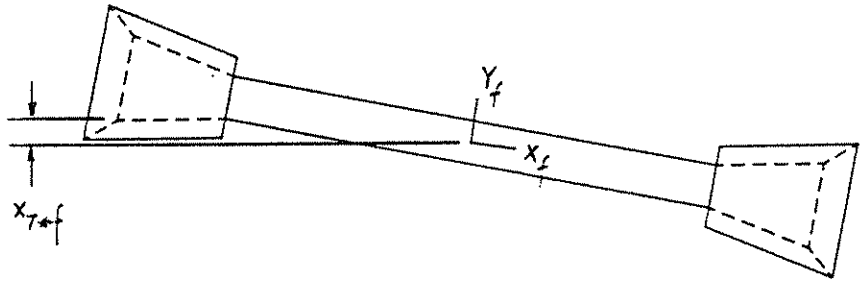

Case 1: $x_{7*f} > 0$

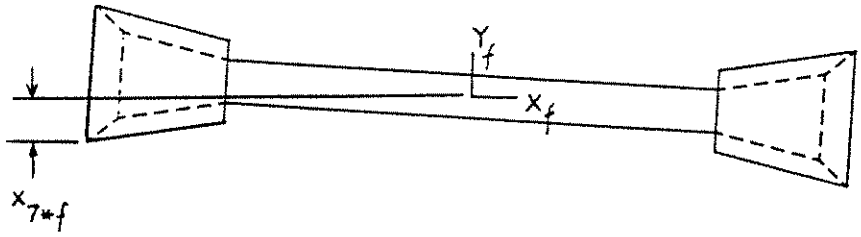

Case 2 : $x_{7*f} < 0$

Fig. 10 : Stability conditions of the beam

4.2 FORCE AND MOMENT ANALYSIS IN STAGE I

Force and moment analysis is used to obtain the compliance of the connection process and the force/moment carrying requirements of the handling system. The analysis is also used to determine conditions for sliding/rotating contacts.

4.2.1 FORCE ANALYSIS

Condition for sliding/rotating During stage one, point contact type #16 occurs; point 7* of the foot will lay on plane <0167> of the shoe. The forces acting on the beam are illustrated in Fig.11. Force balance gives:

$$F_x = (sim5)f_1 \tag{4}$$

$$F_z = (sim8)f_1 \tag{5}$$

where:

$sim5 = \mu\sin\phi - \cos\phi$

$sim8 = -(\sin\phi + \mu\cos\phi)$

The force $(\cos\phi - \mu\sin\phi)f_1$ creates a moment M_{z1} around Z_f axis which is:

$$M_{z1} = (\cos\phi - \mu\sin\phi)(|y_{7*f}| - |x_{7*f}|\delta z)f_1$$

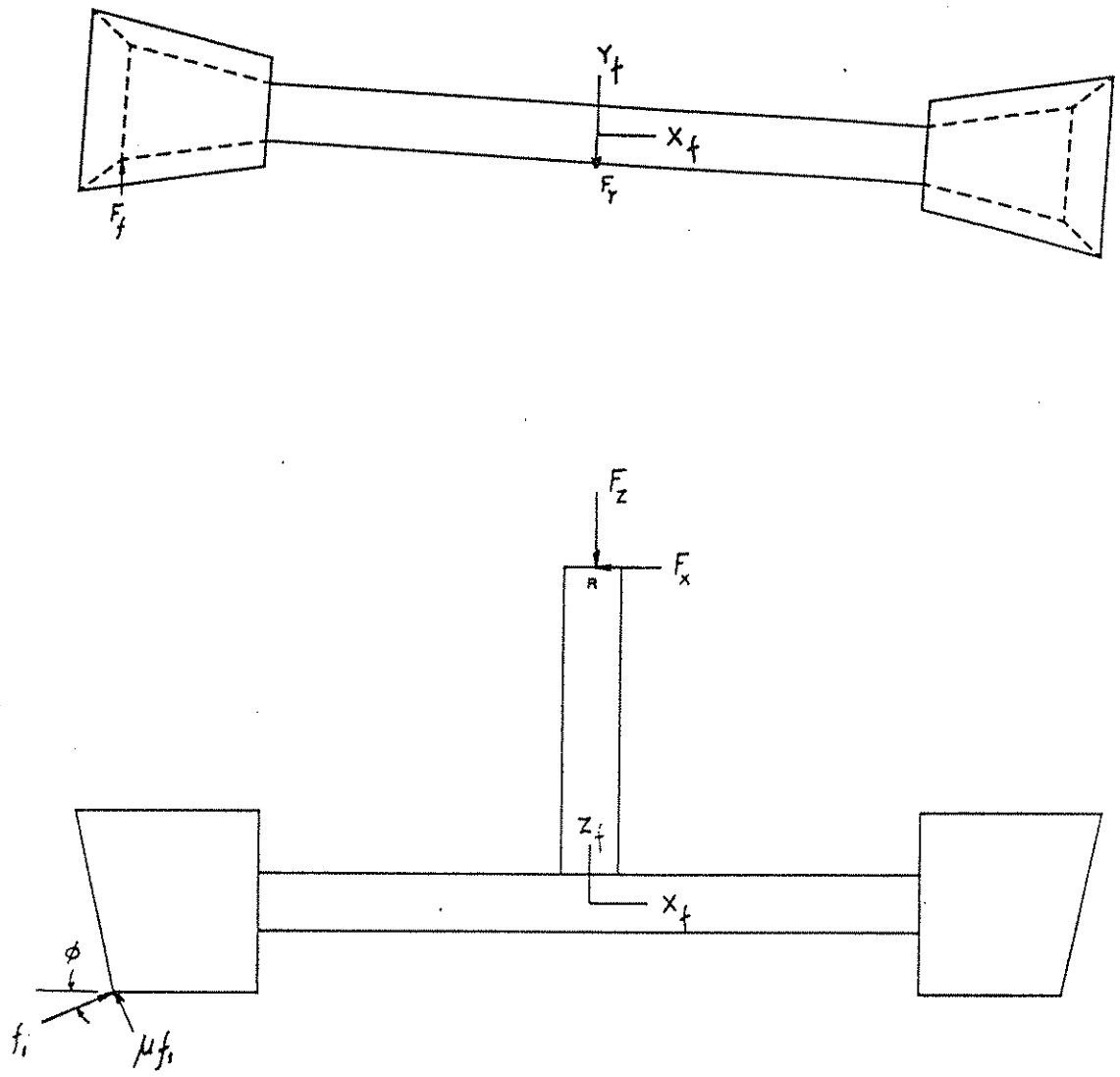

Fig.11 : Force Diagram during Stage One

At the same time, frictional force will develop to oppose the rotation of the beam. The beam will start to rotate when M_{z1} overcomes the static frictional moment or

$$(\cos\phi-\mu\sin\phi)(|y_{7*f}|-|x_{7*f}|\delta z)f_1 \leq \mu|x_{7*f}|f_1 \qquad (6a)$$

We now show even in the best case it is impractical to achieve the inequality (6a). The first of the two terms is maximized when the angles ϕ and δz are small. Inequality (6a) then reduces to:

$$|y_{7*f}| \leq \mu|x_{7*f}| \qquad (6b)$$

For sliding steel on steel μ=0.7 [6], and the length of the beam chosen to be 20 feet, inequality (6b) requires $|y_{7*f}|$ to be the impractical size of at least 84" for rotation to occur. The beam will only slide down on the plane <0167>, no rotation around the Z_f axis occurs.

Forces on handling system The frictional force must be smaller or equal to μf_1. It is determined using equation (6a) and substitute F_f for μf_1:

$$|x_{7*f}|F_f = (\cos\phi-\mu\sin\phi)(|y_{7*f}|-|x_{7*f}|\delta z)f_1 \qquad (7)$$

From (7):

$$F_y = -F_f = (\cos\phi-\mu\sin\phi)(|y_{7*f}|/|x_{7*f}|-\delta z)f_1$$

Combining (4),(5) and (8), there is:

$$\frac{F_x}{F_z} = \frac{sim5}{sim8} \qquad (9)$$

and

$$\frac{F_y}{F_z} = \frac{sim5}{sim8} \quad \frac{|y_{7*f}|}{|x_{7*f}|} - \delta z \qquad (10)$$

These force ratios indicate the force on the handling system that results when exerting an insertion force of F_z. Fig.12 and 13 show how the force ratio varies with the shoe/foot geometric design angle ϕ and friction coefficient

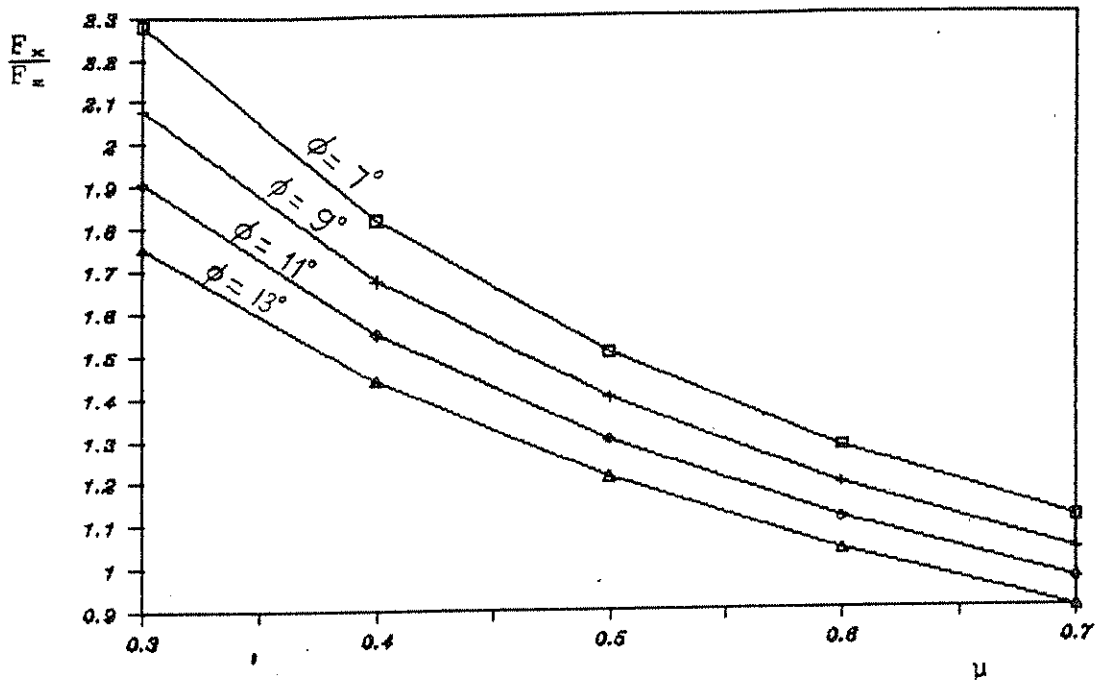

Fig.12 : Fx/Fz v.s. μ and ϕ; Stage One

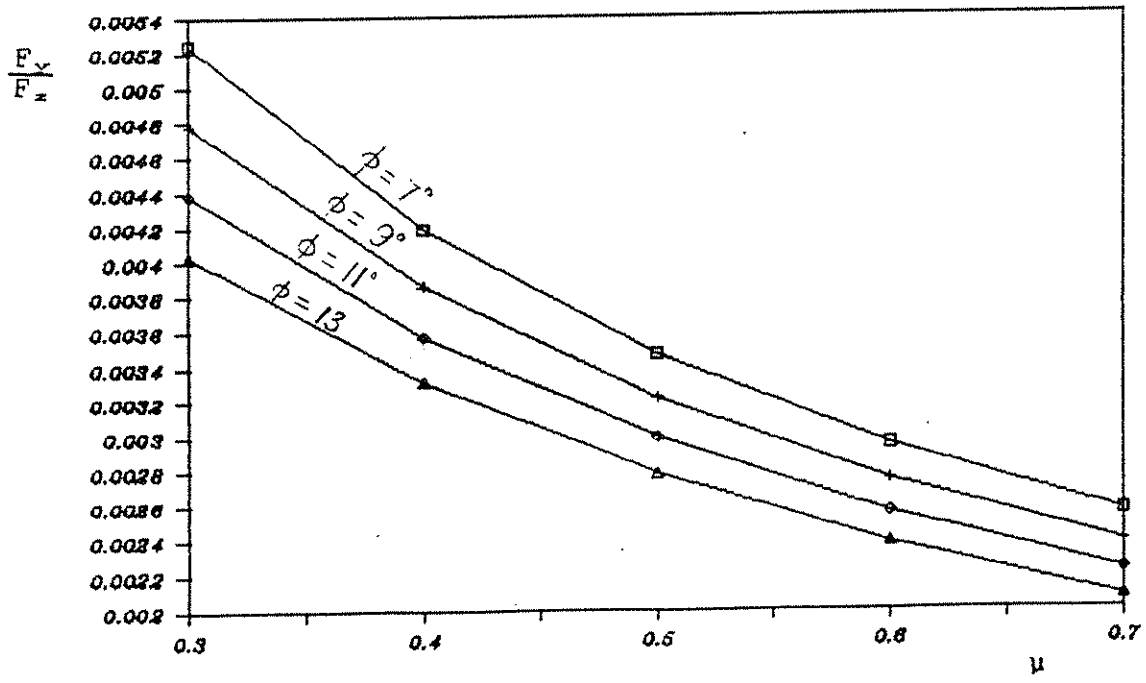

Fig.13 : Fy/Fz v.s. μ and ϕ; Stage One

μ. Both the forces in the x and y directions are inversely proportional to the friction coefficient μ and the angle ϕ. F_y is very small compared to the forces F_x and F_z in this stage.

Stiffness From Fig.1, note that $F_x = -K_x d_x$. The displacement d_x is related to d_z by the shoe/foot geometric design angle ϕ. With the aid of Fig.14, $d_x = -\tan\phi \; d_z$. From equation (9) the joint stiffness $K_{z/x}$ is derived:

$$\frac{F_z}{K_x} = (K_{z/x})d_z$$

where $K_{z/x} = (\text{sim8}/\text{sim5})\tan\phi$.

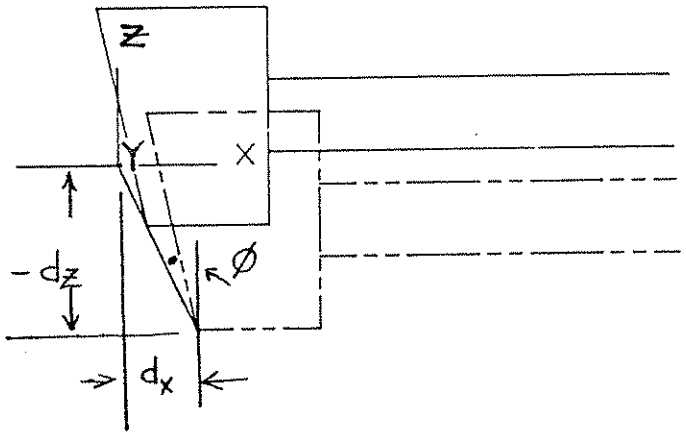

Fig.14 : Geometric Relationship between dx and dz

The resulting stiffness is the slope of the line created by plotting F_z/K_x vs d_z as shown in Fig.15. Different values of ϕ and μ are used in Fig.16 to see how

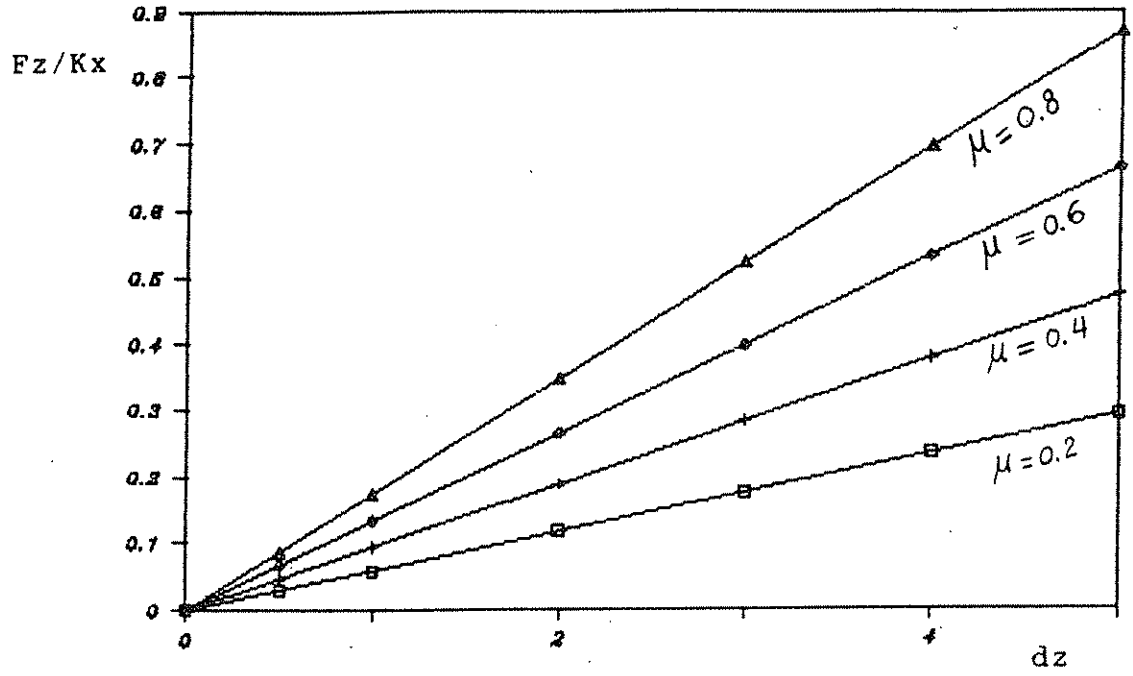

Fig.15 : Fz/Kx v.s.μ and dz; Stage One

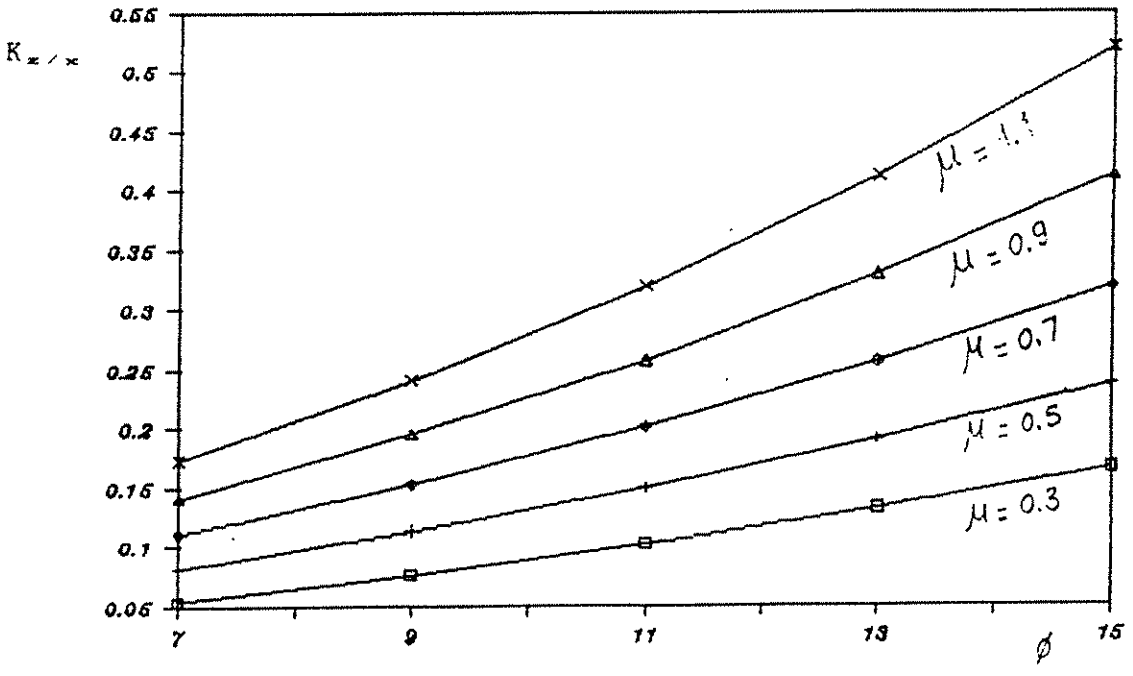

Fig.16 : Kz/x v.s. μ and Ø ; Stage One

the stiffness varies with design parameters. The stiffness increases with the friction coefficient as expected. The stiffness also increases as angle ϕ gets bigger.

4.2.2 MOMENT ANALYSIS

Using moment balance equations about point R and Fig. 11:

- $M_{xf} = -[-(|z_{7*f}|+d)F_y+|y_{7*f}|F_z]$ (11a)
- $M_{yf} = -[(|z_{7*f}|+d)F_x-|x_{7*f}|F_z]$ (11b)
- $M_{zf} = 0$ (11c)

Combining equation (11a) with equation (10) and equation (11b) with equation (9) results in:

$$\frac{M_{xf}}{F_z} = \frac{sim5}{sim8}\frac{|y_{7*f}|}{|x_{7*f}|} - \delta z\,(|z_{7*f}|+d)-|y_{7*f}| \qquad (12a)$$

and:

$$\frac{M_{yf}}{F_z} = -\frac{sim5}{sim8}(|z_{7*f}|+d)+|x_{7*f}| \qquad (12b)$$

Equations (12a) and (12b) are plotted in Fig.17 and Fig.18 using different values of d. All the moment-force ratios are inversely proportional to the handling system length d. M_x/F_z is much smaller than M_y/F_z because the force F_y is small in this stage.

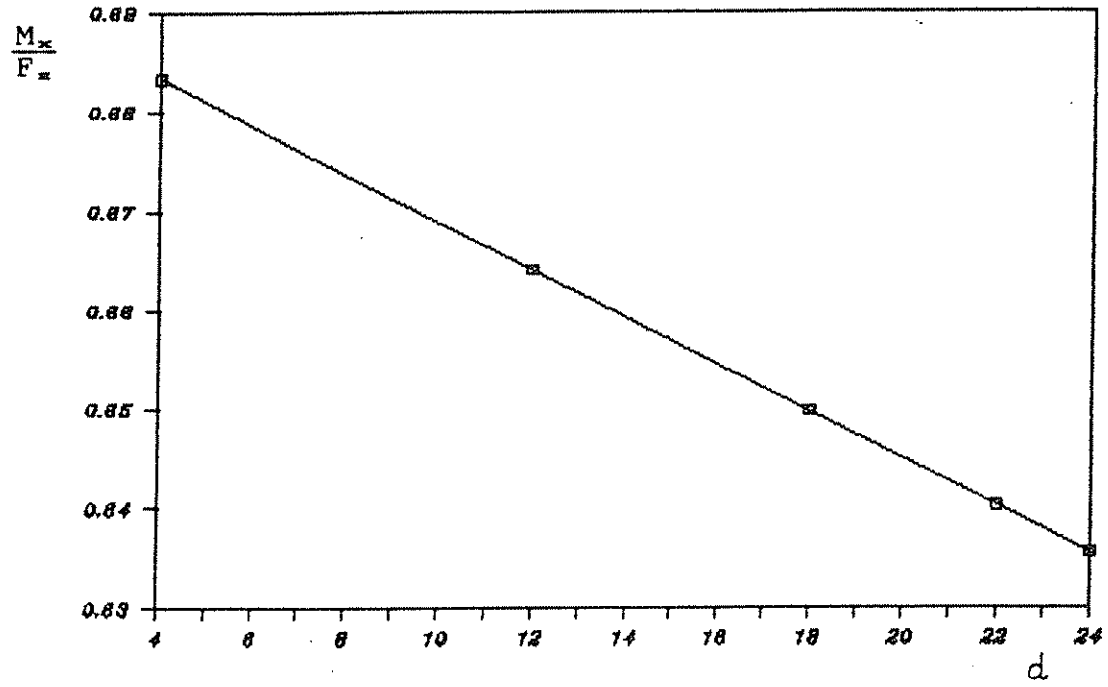

Fig.17 : Mx/Fz v.s. d; Stage One

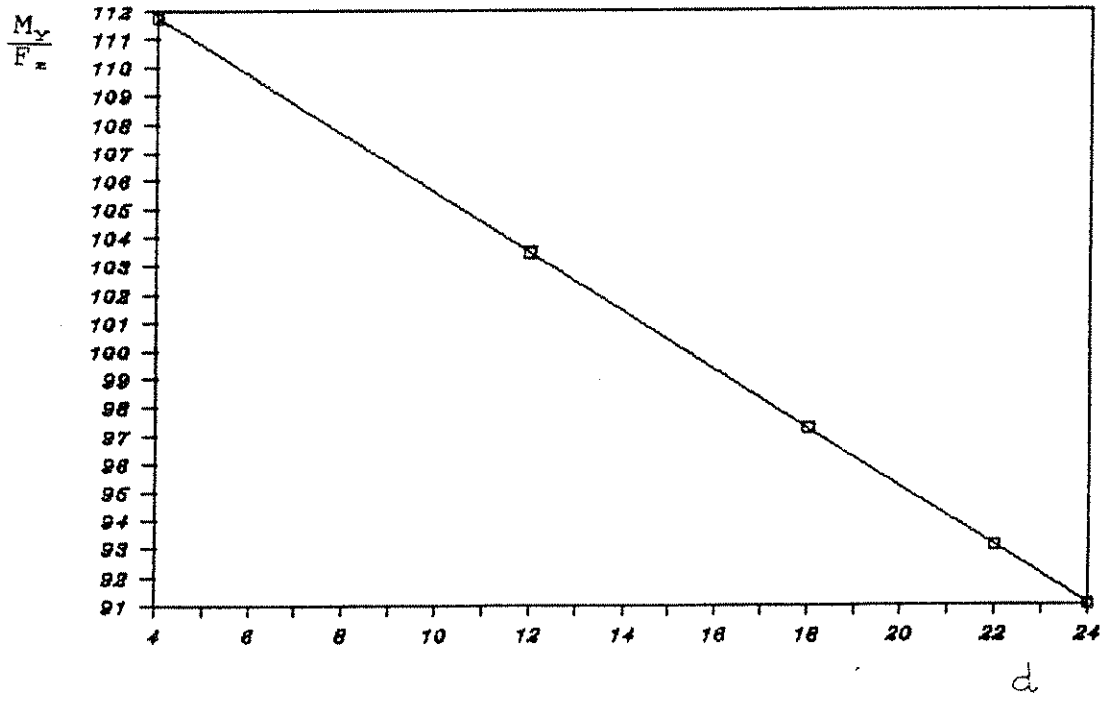

Fig.18 : My/Fz v.s. d; Stage One

4.3 TRAJECTORY OF THE BEAM

Initial contact point. The coordinates of the initial contact point are needed for later calculations to determine the trajectory of the beam. They are obtained by writing an expression for the coordinates of corner 7* in the shoe coordinate system and deriving at what value of the insertion variable z, the corner 7* coordinates are equal to those of the plane <0167>. The equation of the plane is:

$$x + (\tan\phi)z = 0$$

while the x,y,z values of point 7* in the shoe coordinate system are calculated from equation (1). The resulting intersection occurs when :

$$z_{7*} = \frac{x_{7*a}}{\tan\phi}$$

Trajectory. The trajectory of the beam is defined by the trajectories of point 7* and point 7". The coordinates of points 7* and 7" at the end of stage one, 7^*_1, $7"_1$, are directly related to the amount of movement of the beam in the z direction, d_{z1}, in that period. To find d_{z1} we first obtain the coordinates of point contact #53.

The new coordinates of corners 0" and 7" at the end of stage one are found from the geometry relationship $d_x = -(\tan\phi)d_z$ found before:

$$x_{7"i} = x_{7"a} - (\tan\phi)d_{z1}$$
$$y_{7"i} = y_{7"a} \qquad (13)$$
$$z_{7"i} = z_{16} + d_{z1}$$

$$x_{0"I} = x_{0"a} - (\tan\phi)d_{z1}$$
$$y_{0"I} = y_{0"a} \qquad (14)$$
$$z_{0"I} = z_{16} + c + d_{z1}$$

where $x_{0"a}$, $y_{0"a}$, $z_{0"a}$...are the coordinates of corner 0",...in the shoe coordinate system.

Using equations (13) and (14), we find the equation of line 0"7" at the end of stage one:

$$\frac{x-(x_{0"a}-\tan\phi d_{z1})}{(x_{7"a}-x_{0"a})} = \frac{y-(y_{0"a})}{(y_{7"a}-y_{0"a})} = \frac{z-(z_{16}+c+d_{z1})}{-c} \qquad (15)$$

Point contact type #53 occurs on the line 0´3´, where the z coordinate is zero. Thus equation (15) reduces to:

$$x = sim99 + sim98\,d_{z1} \qquad (16)$$

$$y = sim97 + sim96\,d_{z1} \qquad (17)$$

where:

$$sim99 = \frac{(x_{7"a}-x_{0"a})(z_{16}+c)}{c} + x_{0"a}$$

$$sim98 = \frac{(x_{7"a}-x_{0"a})}{c} - \tan\phi$$

$$sim97 = \frac{(y_{7"a}-y_{0"a})(z_{16}+c)}{c} + y_{0"a}$$

$$sim96 = \frac{(y_{7"a}-y_{0"a})}{c}$$

The above values of x and y must also satisfy the equation of line 0´3´ or :

$$y = (-\tan\alpha)x+(L+2b)\tan\alpha \qquad (18)$$

Substituting for x and y in equation (18) from equation (16) and (17) results in:

$$sim97+sim96d_{z1} = (-\tan\alpha)(sim99+sim98\ d_{z1})+(L+2b)\tan\alpha$$

The value of d_{z1} is then determined by:

$$d_{z1} = \frac{(L+2b)\tan\alpha-sim97-\tan\alpha sim99}{sim96+\tan\alpha sim98} \qquad (19)$$

The trajectories of points 7* and 7" are shown in Fig.19. The plot shows that the position errors of both ends of the beam are reduced as the insertion in the z direction progresses.

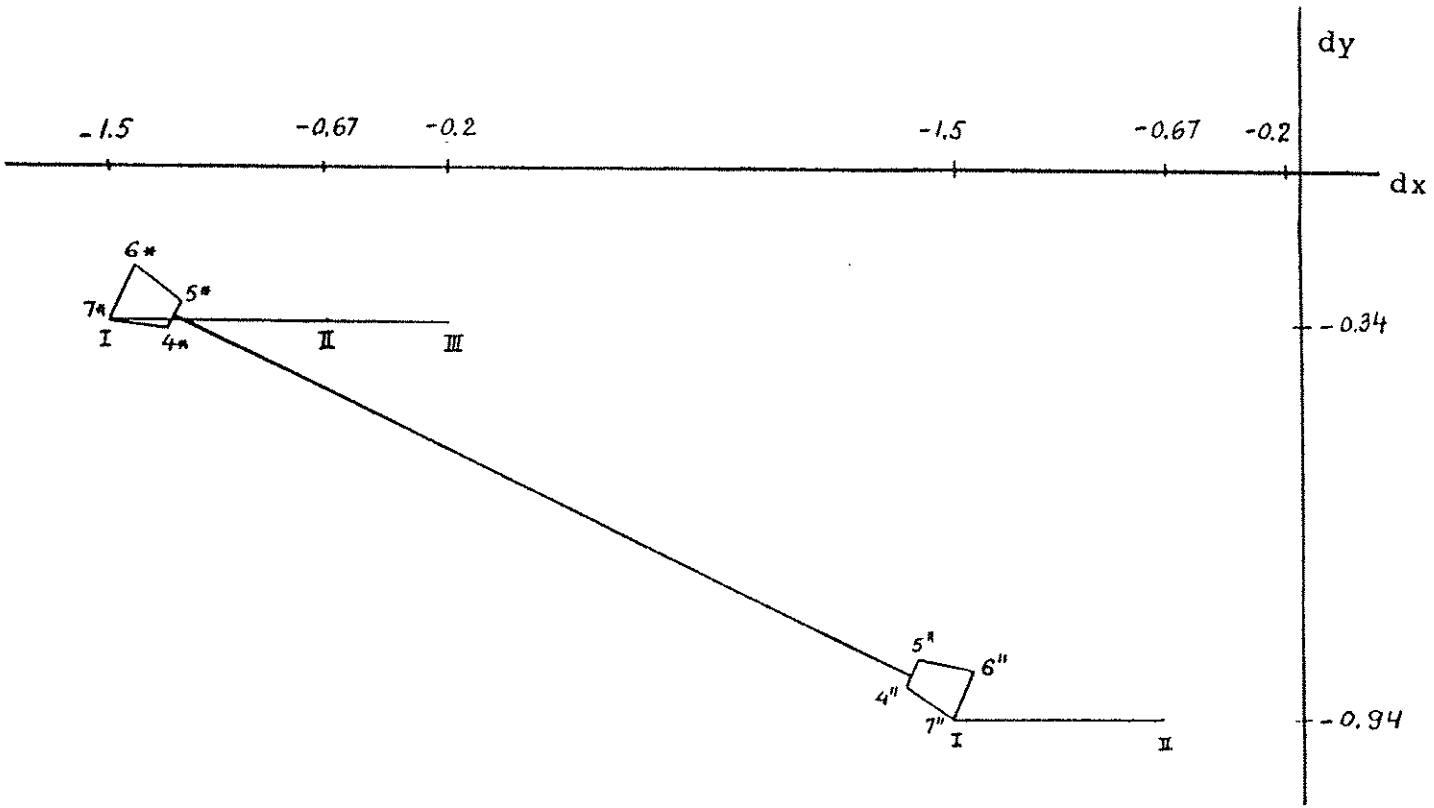

Fig.19 : Trajectories of Points 7* and 7"; Stage One

5. SECOND STAGE ANALYSIS

In this stage, the edge 3´0´of the right shoe slides on the edge 0"7"of the right foot. On the left side, the corner 7* can travel in one of two different trajectories. It can slide down on the plane <0167> with or without simultaneously rotating around Z_f.

In order to determine which of the two trajectories is most desirable, we perform the following analysis. First, the geometrical relationship between the feet and shoes are determined. Second, a force analysis is completed. The condition for the rotating and the pure sliding trajectories of the beam is then derived. The forces acquired from the two trajectories are compared and one trajectory is chosen for detailed analysis. The stiffness of the connection is obtained through geometrical equations and kinematic equations. Third, moment analysis is performed. Finally, the trajectory of the beam is determined.

5.1 GEOMETRICAL ANALYSIS

In this section we find the relationships between the beam motions d_x,d_y and d_z during the second stage insertion.

Movement in the x direction

As the beam moves down, it is constrained by the side of the foot to move in the x direction by an amount determined from Fig.14:

$$d_x = -(\tan\phi)d_z \tag{20}$$

Movement in the y direction

The total movement in the y direction is the sum of the movements caused by the simultaneous sliding on the 0"7" edge and the 0´3´ edge. To derive the total movement we first determine the motion along the 0"7" edge and then add to it the motion along the 0´3´ edge.

An equation of the line 07 describes the relationship between d_y and d_z for the first of these sliding motions. Line 07 occurs at the intersection of the planes <0167> and <0347>:

$$y+(\tan\alpha\tan\phi+\tan\tau)z = 0$$

When the beam goes down an amount of d_z, it thus translates in the y direction by an amount:

$$d_{y1} = -(\tan\alpha\tan\phi+\tan\tau)d_z \tag{20a}$$

The second sliding motion which occurs on 0´3´ also causes the beam to move in the -y direction by an amount

$$d_{y2} = -(\tan\alpha)d_x = (\tan\alpha\tan\phi)d_z \qquad (20b)$$

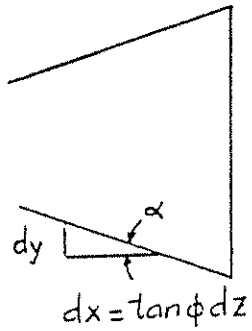

Fig.20 : Geometric Relationship between dy and dz

Total movement in the y direction is found from equations (20a) and (20b) to yield:

$$d_y = d_{y1}+d_{y2} = -(\tan\tau)d_z \qquad (21)$$

5.2 FORCE ANALYSIS

We next determine the forces on the beam during the insertion. This information is later used to find the forces on the handling system and the conditions for sliding and rotating of the left foot.All of the forces acting on the beam are shown in Fig.21. The total reaction forces in the x,y,z directions of the right foot and the left foot are expressed as:

$$F_{L2X} = -(\sin 5)f_{12} \qquad (22)$$

$$F_{L2Y} = F_f \qquad (23)$$

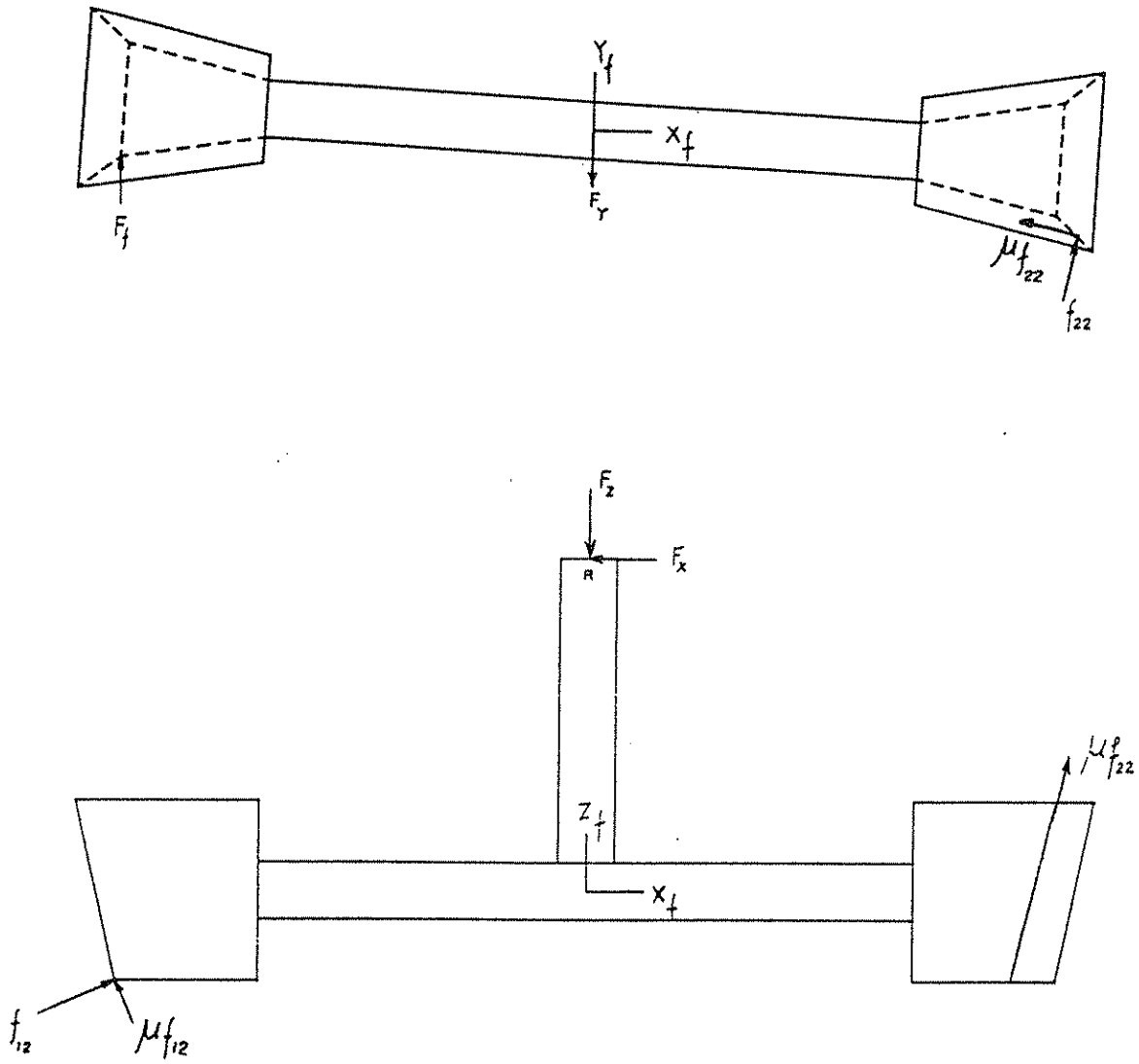

Fig.21 : Force Diagram during Second Stage

$$F_{L2Z} = -(sim8)f_{12} \quad (24)$$

$$F_{R2X} = -(sim26)f_{22} \quad (25)$$

$$F_{R2Y} = -(sim27)f_{22} \quad (26)$$

$$F_{R2Z} = -(sim28)f_{22} \quad (27)$$

where F_f is the frictional force and:

$$sim25 = bc\ (1+(\tan\alpha)^2+(\tan\tau)^2)$$

$$sim26 = \mu\cos\alpha-\mu\cos\tau\sin\phi - \frac{bc\tan\alpha}{sim25}$$

$$sim27 = \mu\sin\tau-\mu\sin\alpha - \frac{bc}{sim25}$$

$$sim28 = -\mu\cos\tau\cos\phi - \frac{bc\tan\tau}{sim25}$$

A force balance on the beam yields:

$$F_x = (sim5)f_{12}+(sim26)f_{22} \quad (28)$$

$$F_y = -F_f+(sim27)f_{22} \quad (29)$$

$$F_z = (sim8)f_{12}+(sim28)f_{22} \quad (30)$$

From equations (28) and (30), the normal reaction forces f_{12} and f_{22} are derived in terms of F_x and F_z as:

$$f_{12} = (sim45)F_z \quad (31)$$

$$f_{22} = (sim44)F_z \quad (32)$$

where:

$$sim33 = \frac{sim5sim28 - sim8sim26}{sim5}$$

$$sim44 = \frac{1}{sim33} - \frac{sim8(F_x/F_z)}{sim5sim33}$$

$$sim45 = \frac{sim33 - sim28}{sim8sim33} + \frac{sim28(F_x/F_z)}{sim5sim33}$$

The right foot will loose contact with the right shoe when f_{22} which is determined by sim44, becomes zero. That occurs when F_x/F_z equals to 1.05. This is the maximum value of F_x/F_z for the beam to continue to move down in the second stage of the insertion. If F_x/F_z exceeds 1.05, F_x will force the beam against the plane <0167>. F_z will not be great enough to drive the beam down and consequently jamming will occur.

The actual frictional force F_f of the left foot against the left shoe is found by the moment balance around Z_f axis:

$$|x_{7*f}|F_f = (|y_{7*f}| - |x_{7*f}|\delta z)F_{L2X} + (x_{53} - ((L/2)+b+dx+d_{x1})F_{R2Y} - ((b/2)+dy-|y_{53}|)F_{R2X} \quad (33)$$

Combining equations (22),(25),(26) with equation (33) we obtained:

$$F_f = -\frac{sim43}{|x_{7*f}|} f_{12} + \frac{sim42}{|x_{7*f}|} f_{22} \qquad (34a)$$

where:

$$sim42 = sim26((b/2)+dy-|y_{53}|)-sim27(x_{53}((L/2)+b+dx+d_{x1})$$

$$sim43 = sim5(|y_{7*f}|-|x_{7*f}|\delta z)$$

The beam will not rotate around Z_f axis when F_f is smaller than the maximum allowable static frictional force on the left side or

$$F_f < \mu f_{12} \qquad (34b)$$

Equation (34b) can be reduced by combining it with equations (31),(32) and (34a):

$$sim42sim44-(sim43+\mu|x_{7*f}|)sim45 > 0 \qquad (34c)$$

For any set of dimensional parameters, the left side of the inequality depends only on the ratio F_x/F_z. Substituting various values for F_x/F_z into equation (34c) we find the following:

$$0 < \frac{F_x}{F_z} < 0.3 : \quad \text{rotating}$$

$$0.3 < \frac{F_x}{F_z} < 1.05 : \quad \text{sliding}$$

For each of these two types of motions, different sets of force expressions apply. In the case of sliding, the

relationship between the forces is obtained by substituting the values of f_{12},f_{22}, F_f from equations (31),(32),(34a) into equation (29):

$$F_y = (sim48)F_z+(sim49)F_x \tag{35}$$

or:

$$\frac{F_y}{F_z} = sim48 + sim49\,\frac{F_x}{F_z} \tag{36}$$

where:

$$sim48 = \frac{sim47}{sim33} + \frac{sim46(sim33-sim28)}{sim8sim33}$$

$$sim49 = \frac{sim28sim46}{sim5sim33} - \frac{sim8sim47}{sim5sim33}$$

The relationship between the forces in the case of rotating is derived similarly but with F_f replaced by μf_{12} in equation (29). After carrying out the same calculations, we have:

$$\frac{F_y}{F_z} = sim27sim44-\mu sim45 \tag{37}$$

Both equations (36) and (37) are plotted in Fig.22. The region where F_x/F_z is negative, not shown in the figure, represents the withdrawal process of the beam from the shoe. As long as F_x/F_z is positive and smaller than 0.3, the beam rotates around the Z_f axis. In this latter case the force ratio F_y/F_z is high and relatively constant.

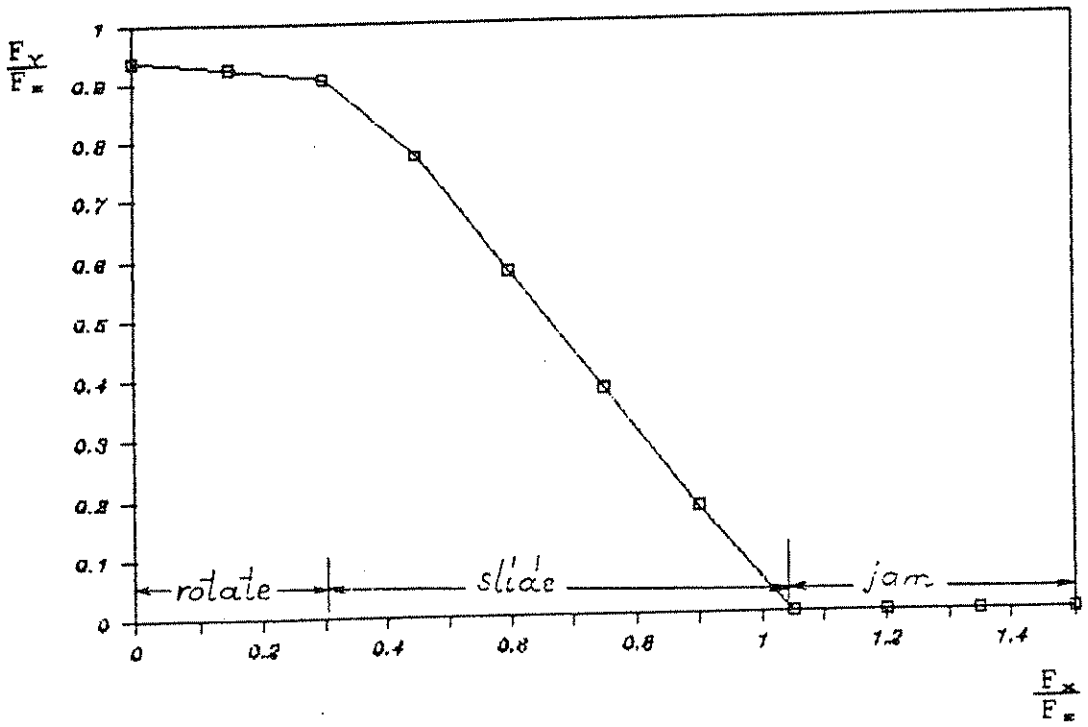

Fig.22 : Conditions for Rotating and Sliding

The beam will start to slide down when F_x/F_z exceeds 0.3 . As F_x/F_z increases, F_y/F_z decreases rapidly and the beam will be harder to push. Finally when F_x/F_z is greater than 1.05, the beam is jammed against the left shoe and the insertion stops.

We select the sliding trajectory for the subsequent detailed analysis. The selection of this trajectory is based on two reasons. First, this trajectory has a wider range of F_x/F_z, therefore it is easier to maintain during the insertion process. Second, smaller value of F_y/F_z can be obtained, so that no additional rigidity of the handling

system in the y direction is required.

Connection stiffness The stiffness of the connection is obtained by combining the geometrical equations with the force equations.

Geometrical equations

$$d_x = -\tan\phi \; d_z$$

$$d_y = -\tan\tau \; d_z$$

Force equations

$$F_x = -K_x d_x$$ Handling system connection

$$F_y = -K_y d_y$$ force-displacement equations

$$F_y = (\text{sim48})F_z + (\text{sim49})F_x \tag{35}$$

Combining all of the above equations yields the shoe-foot force displacement equation:

$$\frac{F_z}{K_x} = \left[\frac{K_y}{K_x} \frac{\tan\tau}{\text{sim48}\tan\phi} - \frac{\text{sim49}}{\text{sim48}} \tan\phi \right] d_z \tag{38}$$

The bracket term represents the connection stiffness. The stiffness depends on the handling system stiffness and increases with K_y/K_x (Fig.23). Fig.24 superimposes the stiffness plot of the first stage and the stiffness plot of the second stage when K_y/K_x equals to 0.4. The slope of the plot increases at the transition where second stage starts.

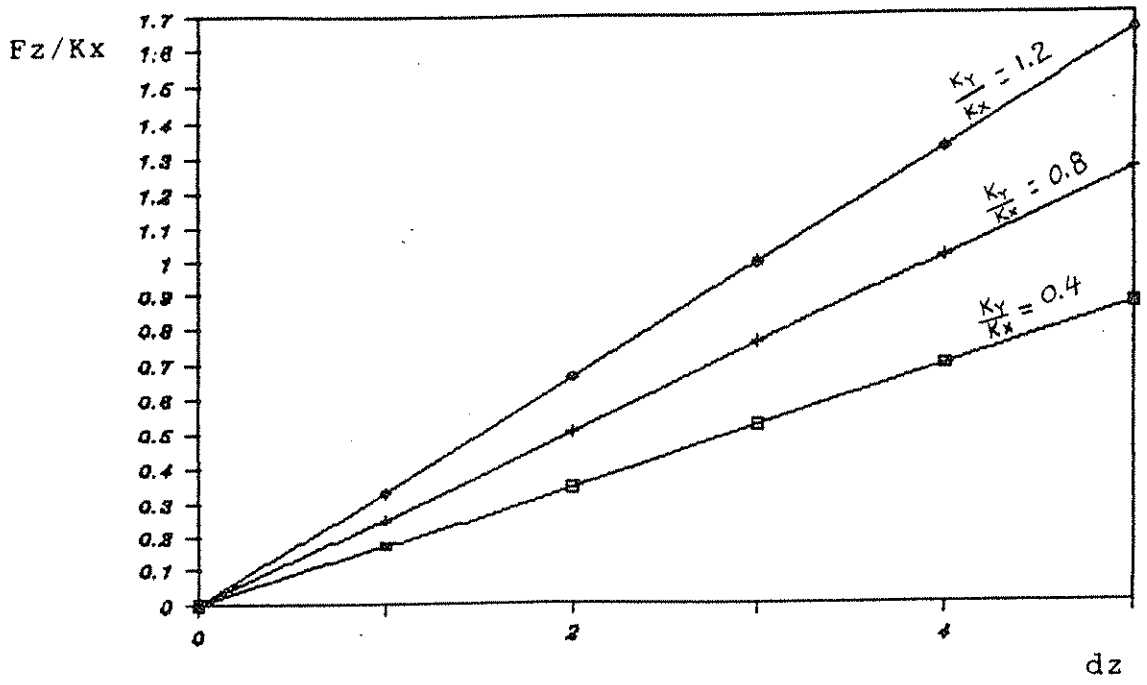

Fig.23 : Fz/Kx v.s. dz and Ky/Kx; Stage Two

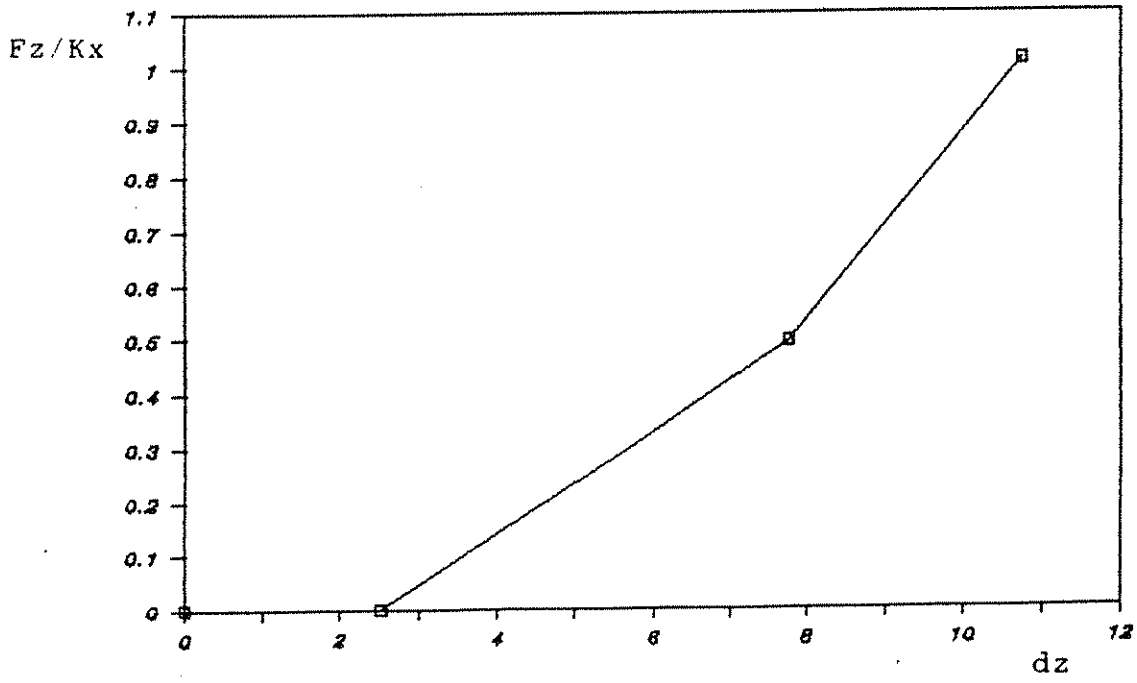

Fig.24 : Connection Stiffness; Stages One and Two

5.3 MOMENT ANALYSIS

The moments on the handling system are determined using the moment balance equations around point R. From Fig.25 we have:

$$M_x = -(sim51-d_z)F_{R2Y}+(sim52+tan\alpha tan\phi d_z) -F_f(d+|z_{7*f}|)F_{R2Z}+|y_{7*f}|F_{L2Z}$$

where:

$$sim51 = d-((c/2)-z_{16}-d_{z1})$$

$$sim52 = b+dy-y_{53}$$

where d_z is the movement in the z direction in stage two.

Replacing F_{L2Z}, F_{R2Y}, F_{R2Z}, and F_f with expressions given in equations (24),(26),(27) and (34a) and combining it with the equations (31) and (32) gives:

$$\frac{M_x}{F_z} = -sim28sim44(sim52+tan\alpha tan\phi d_z) +sim27sim44(sim51-d_z)-sim50(d+|z_{7*f}|)-sim8sim45$$

The moment M_y is determined similarly to yield:

$$M_y = -(sim51-d_z)F_{R2X}+(sim53-tan\phi d_z) -|x_{7*f}|F_{L2Z}+F_{L2X}(d+|z_{7*f}|)F_{R2Z}$$

where $sim53 = x_{53}-x_p-dx-d_{x1}$

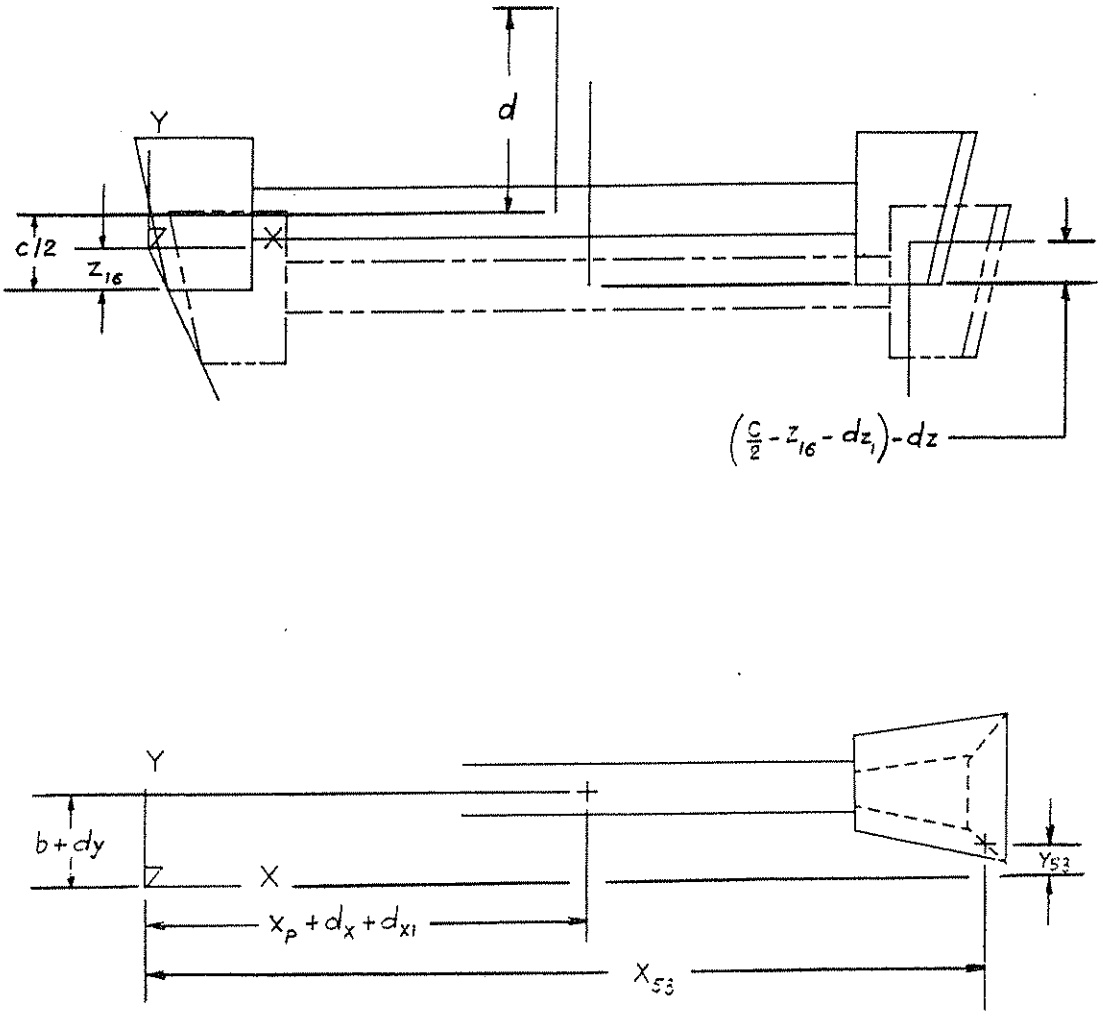

Fig.25 : Moment Arms; Stage Two

Replacing values of $F_{L2X}, F_{L2Z}, F_{R2X}, F_{R2Z}$ from equations (22),(24),(25),(27) into the above equations and combining it with equations (31) and (32), we have:

$$\frac{M_y}{F_z} = sim26sim44(sim51-d_z)-sim28sim44(sim53-tan\phi d_z)$$
$$-sim5sim45(d+|z_{7*f}|)+sim8sim45|x_{7*f}|$$

The moment-force ratios M_x/F_z and M_y/F_z depend on three values; F_x/F_z, d_z and d. Their relationships are shown in Figs.26,27,28,29. In general, both M_x/F_z and M_y/F_z are inversely proportional with F_x/F_z, d_z and directly proportional with d.

5.4 TRAJECTORY OF THE BEAM

During the second stage, corner 6* rotates around corner 7* by δ_{y2} while it descends down d_{z2}. The end of stage two occurs when corner 6* contacts the plane <1256> in point contact #34. The coordinates of corner 6* at the end of the stage two trajectory are determined by first finding the coordinates of point 6* at the end of stage 1 from:

$$x_{6*1} = x_{6*a}-tan\phi d_{z1}$$
$$y_{6*1} = y_{6*a}$$
$$z_{6*1} = z_{6*a}+d_{z1}$$

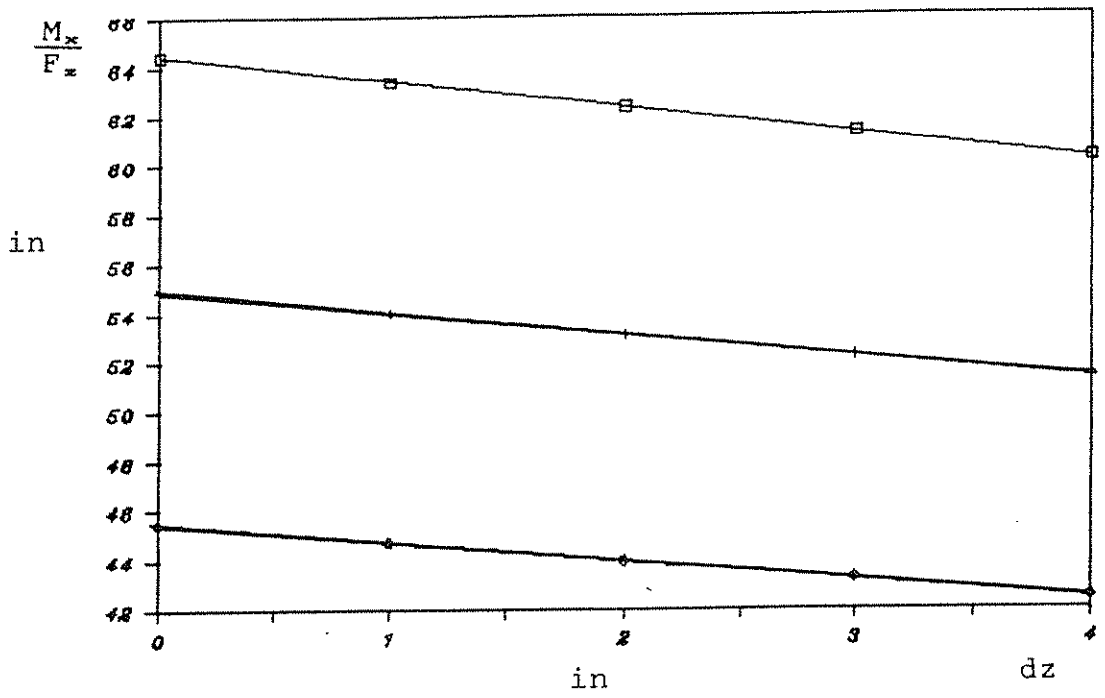

Fig.26 : Mx/Fz v.s. Fx/Fz, dz and d=30"; Stage Two

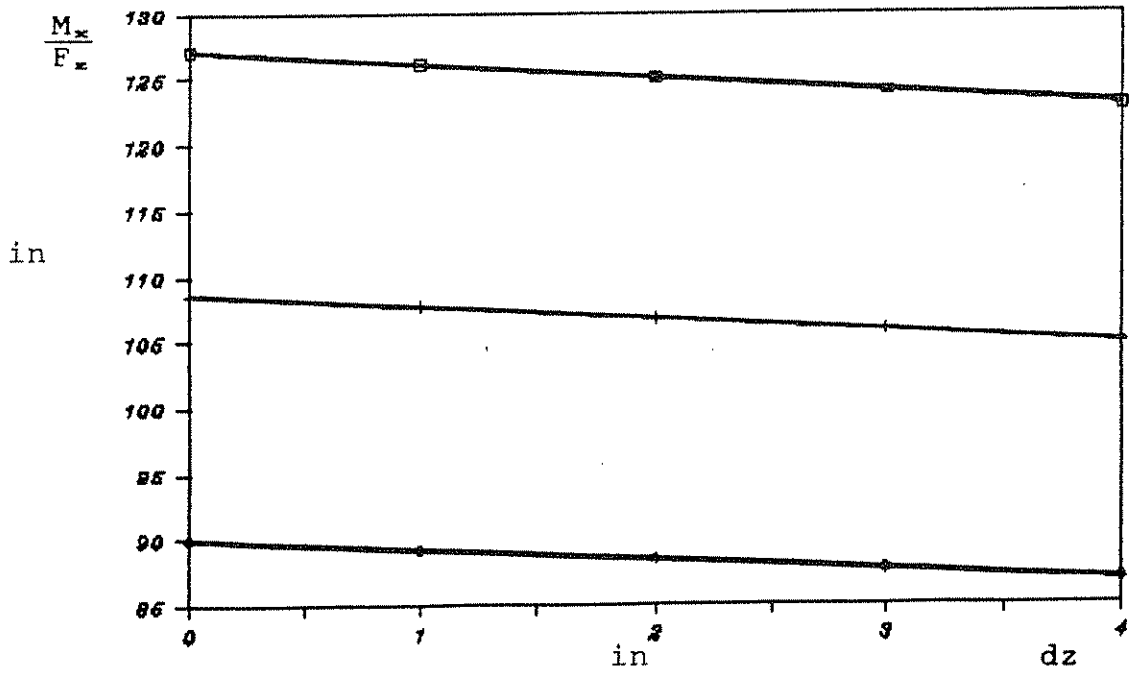

Fig.27 : Mx/Fz v.s. Fx/Fz, dz and d=60"; Stage Two

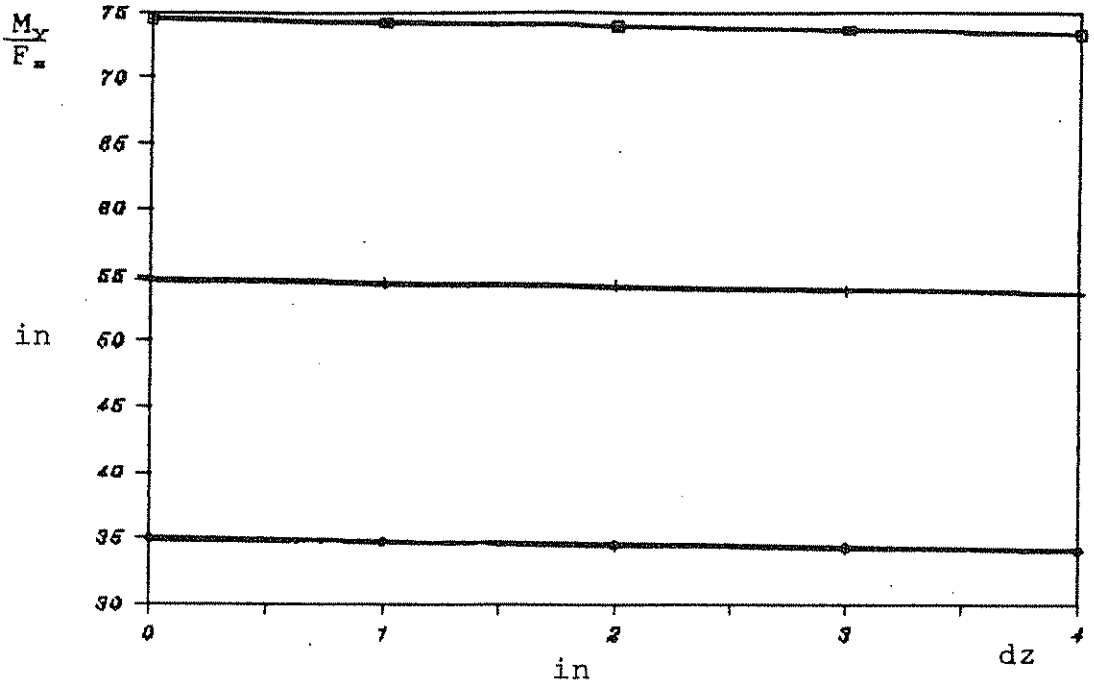

Fig.28 : My/Fz v.s. Fx/Fz, dz and d=30"; Stage Two

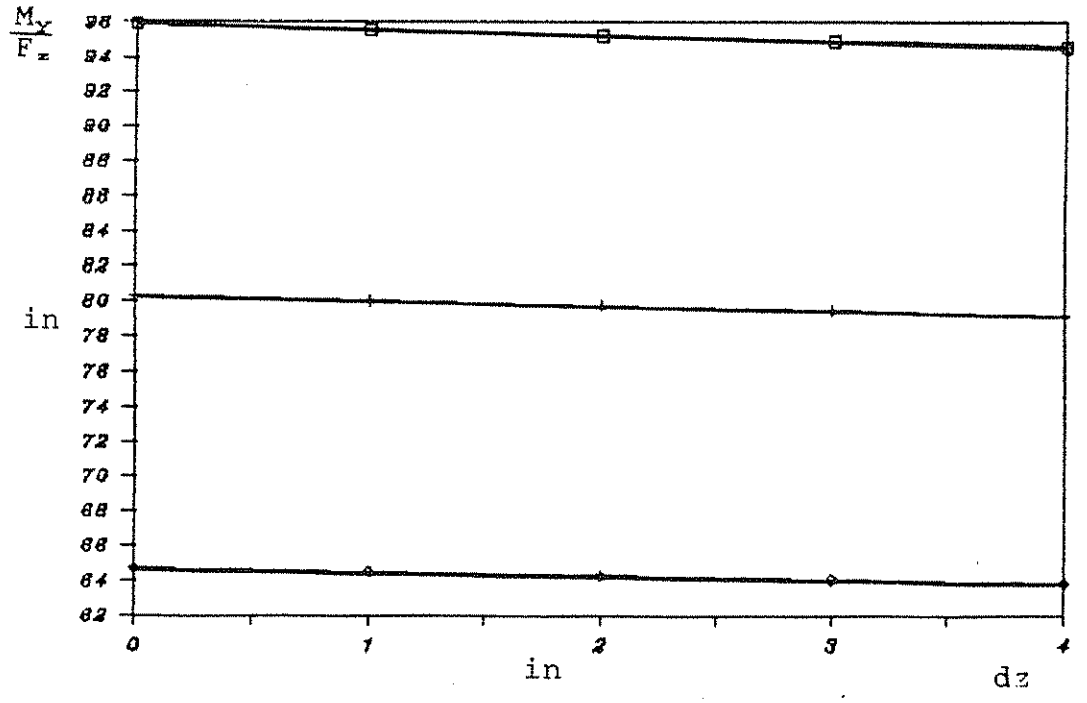

Fig.29 : My/Fz v.s. Fx/Fz, dz and d=60"; Stage Two

and then assuming that both δ_{y2} and d_{z2} are small resulting in:

$$\begin{aligned} x_{6*2} &= x_{6*1} - \tan\phi d_{z2} \\ y_{6*2} &= y_{6*1} \\ z_{6*2} &= z_{6*1} + d_{z2} \end{aligned} \tag{39}$$

Corner 6*, at the end of stage two motion, must also lay on the plane <1256>. The normal vector defining the plane is in the direction of 12 X 16. The plane also contains point 1*. The equation of the plane is thus:

$$(\tan\alpha)x+(y-a)-(\tan\tau)z = 0 \tag{40}$$

Combining equations (39) and (40) we obtain the amount of movement in the z direction, d_{z2}, during the second stage:

$$d_{z2} = \frac{(\tan\alpha)x_{6*1}+y_{6*1}-a-(\tan\tau)z_{6*1}}{(\tan\alpha\tan\phi+\tan\tau)}$$

At the end of stage two, both corners 7* and 7" travel in the x and z directions by $-\tan\phi\ d_{z2}$ and d_{z2} respectively. Corner 7" also gets closer to its desired y position by an amount of $-\tan\tau\ d_{z2}$. As shown in Fig.30, the position errors approach zero during the first and second stages of the insertion process, with the ends of the stage one trajectory being indicated by I and II and the ends of the stage two trajectory being indicated by II and III. The error in the x direction decreases at the

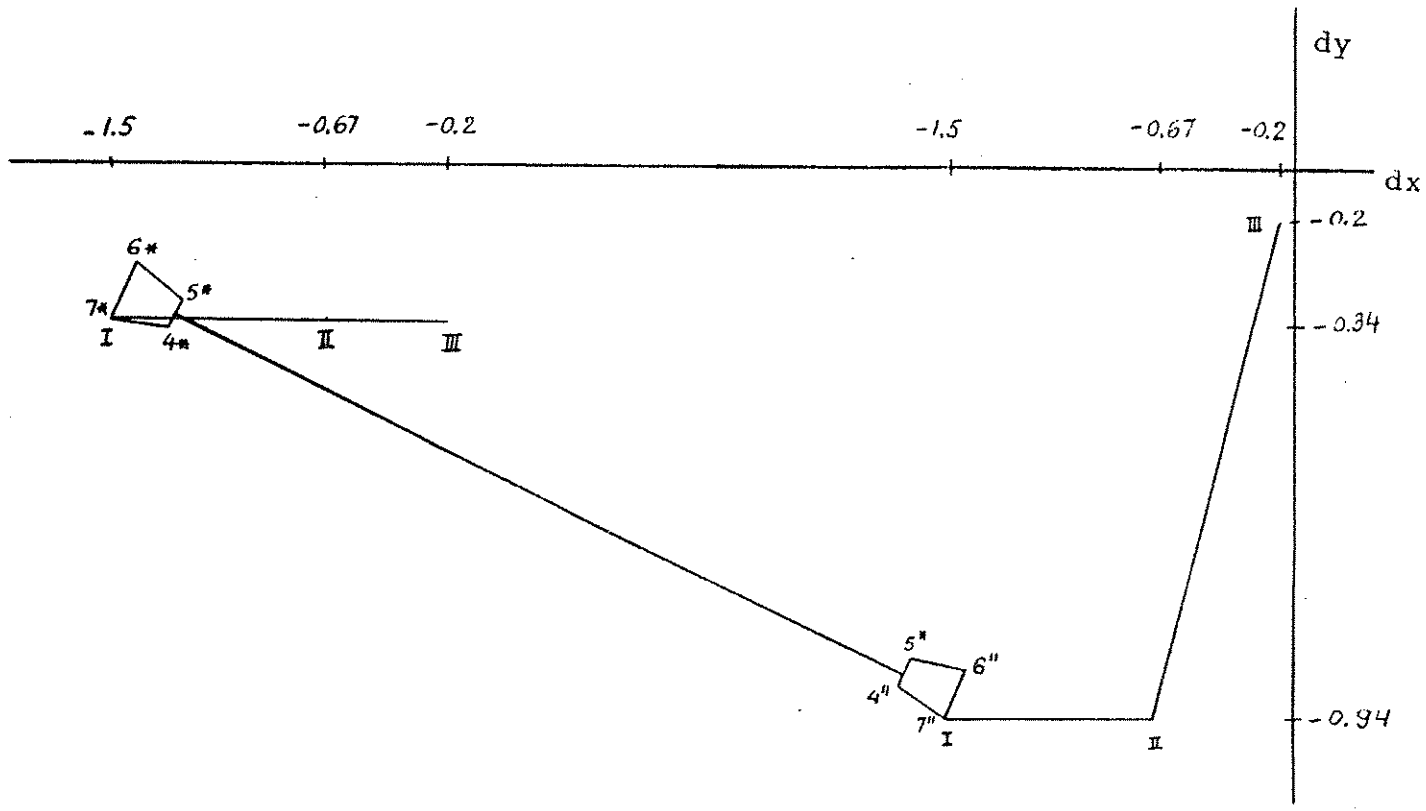

Fig.30 : Trajectories of Points 7* and 7"; Stage Two

same rate for both corners 7* and 7". The rate of which the errors decreases in the y direction are directly related to the types of movement that occurs: sliding on the left side of the beam and pivoting around 7* on the right side.

6. CONCLUSION

The beam-column insertion process, using a chamfered connection design, is a complex and precarious task due to the strict geometrical constraints and a numerous set of trajectories that the beam can have .

1/ There are thirty nine different contact types in the single sided insertion class. The number of contact types in the two sided insertion class is much higher because one contact type can occur on one side of the beam while a different type of contact occurs on the other side. Classes of trajectories are defined by the types of contact that occur during the insertion process. A class of trajectory is well defined as soon as the geometric design parameters are determined and the initial error parameters are known.

2/ The success of an insertion depends heavily on the selection of the geometric design parameters and error variables. For any particular class of trajectories, a range of geometric parameters and error variables are allowed. Given a range of error variables, combinations of the design parameters that will allow a particular class of insertion trajectories can be obtained using equations (2) and (3). The above combinations are further reduced by a stability condition, equation (3.b), of the beam insertion process. For example, the length of the beam is the most

restrictive parameter to initial insertion angle error. The longer the beam, the smaller the allowable initial angle . A longer beam also contributes to the instability of the insertion process. With initial position and orientation error variables of $\delta z=0.3°$, dx=-1.5", dy=-0.3", the following design parameters were obtained based on geometrical constraints: a=8", b=4", c=12", L=20ft., $\alpha=9°$, $\tau=14°$, $\phi=9°$.

3/ The force in the x direction, F_x, in stage one is greater than the insertion force, F_z, because of the small angle ϕ and friction coefficient μ. Even though larger values of ϕ and μ can be used to reduce the force F_x, they will also increase the stiffness of the connection and require an increase in the insertion force F_z.

In the second stage, the value of F_x/F_z will determine the trajectory of the beam as well as determining if jamming occurs. Rotation of the beam around Z_f axis exists as long as F_x/F_z is smaller than 0.3. In this region, the force ratio F_y/F_z is large ,0.9, and constant. When F_x/F_z is greater than 0.3, frictional moment overcomes the reaction moments and the beam will slide down the plane <0167>. F_y/F_z decreases rather rapidly as F_x/F_z increases. When F_x/F_z equals to 1.05, "pinning" or "jamming" occurs and F_y/F_z goes to zero.

4/ The stiffness of the connection in the first stage of the insertion process is directly proportional to the angle ϕ and the friction coefficient μ . The stiffness is higher in the second stage. In the second stage, the stiffness increases with the spring constant ratio Ky/Kx and is a complex function of all the geometric parameters because of the reaction and friction forces that are exerted on the right foot during this portion of the insertion.

5/ The self-aligned ability of the connection is provided by the three "chamfered angles" α, τ and ϕ. In the trajectory studied, the angle ϕ reduces the error of the beam in the x direction. The error in the y direction is lessened by the net result of the angles α and τ. At the end of stage two, the left foot corrected its error in the x direction by 87% , the right foot reduced its error by the same amount in the x direction and 80% in the y direction.

Many of the results obtained during the limited study can be used to generalize the beam-column insertion process. First, the geometrical constraints (equations 2 and 3) still apply no matter what trajectory the beam will take. Compromise should be made between the allowable range of initial position and orientation error variables and geometrical parameters to achieve a successful insertion. Secondly, the stability of the insertion

process should be investigated. Third, to maintain a particular trajectory, the force ratios at the beam to handling equipment must be kept within predetermined ranges. Finally, the stiffness of the connection is greater as the insertion process continues.

7. REFERENCES

[1] Perreira, N.D., Groover, M.P., Doydum C., Smith, R., "A Survey of Robotics Technology in Construction", ATLSS Report No. 87-04, Lehigh University, June 1987.

[2] Perreira, N.D., Doydum, C., " Site Metrology for Automated Framing and Building Deformation", Working Paper, Center for Advanced Technology for Large Structural Systems at Lehigh University.

[3] Perreira, D.N., Blank,G.B., "Automated Framing", Proposals to the National Science Foundation, Lehigh University, June,1987.

[4] Taylor, R.H., Lozano-Perez, T., Mason, M.T., "Automatic Synthesis of Fine-Motion Strategies for Robots", The International Journal of Robotics Research, MIT Press, Vol.3, 1984

[5] Whitney, D.E., "Quasi-Static Assembly of Compliantly Supported Rigid Parts", Journal of Dynamic Systems, Measurements and Control", American Society of Mechanical Engineers, March 1982, Vol.104/65.

[6] University Physics, Sears and Zimonski, Addison Wesley. Also, Machine Handbook.